BUB-1 targets PP2A:B56 to regulate chromosome congression during meiosis I in *C. elegans* oocytes

Laura Bel Borja[1], Flavie Soubigou[1], Samuel J.P. Taylor[1], Conchita Fraguas Bringas[1], Jacqueline Budrewicz[2,3], Pablo Lara-Gonzalez[2,3], Christopher G. Sorensen Turpin[4], Joshua N. Bembenek[5], Dhanya K. Cheerambathur[6], and Federico Pelisch[1,*]

[1] Centre for Gene Regulation and Expression, Sir James Black Centre, School of Life Sciences, University of Dundee. Dundee, DD1 5EH, UK

[2] Ludwig Institute for Cancer Research, San Diego, California, 92093, USA

[3] Department of Cellular and Molecular Medicine, University of California at San Diego, La Jolla, California, 92093, USA

[4] Department of Biochemistry, Cellular and Molecular Biology, University of Tennessee, C211 Walters Life Sciences Building, 1414 Cumberland Avenue, Knoxville, TN 37996, USA

[5] Department of Molecular, Cellular, and Developmental Biology, University of Michigan. 1105 North University Ave., Ann Arbor, MI 48109-1085, USA

[6] Wellcome Centre for Cell Biology & Institute of Cell Biology, School of Biological Sciences, The University of Edinburgh, Edinburgh, EH9 3BF, UK

* Corresponding author: Federico Pelisch (f.pelisch@dundee.ac.uk)

ABSTRACT

Protein Phosphatase 2A (PP2A) is an heterotrimer composed of scaffolding (A), catalytic (C), and regulatory (B) subunits with various key roles during cell division. While A and C subunits form the core enzyme, the diversity generated by interchangeable B subunits dictates substrate specificity. Within the B subunits, B56-type subunits play important roles during meiosis in yeast and mice by protecting centromeric cohesion and stabilising the kinetochore-microtubule attachments. These functions are achieved through targeting of B56 subunits to centromere and kinetochore by Shugoshin and BUBR1. In the nematode *Caenorhabditis elegans* (*C. elegans)* the closest BUBR1 ortholog lacks the B56 interaction domain and the Shugoshin orthologue is not required for normal segregation during oocyte meiosis. Therefore, the role of PP2A in *C. elegans* female meiosis is not known. Here, we report that PP2A is essential for meiotic spindle assembly and chromosome dynamics during *C. elegans* female meiosis. Specifically, B56 subunits PPTR-1 and PPTR-2 associate with chromosomes during prometaphase I and regulate chromosome congression. The chromosome localization of B56 subunits does not require shugoshin orthologue SGO-1. Instead we have identified the kinase BUB-1 as the key B56 targeting factor to the chromosomes during meiosis. PP2A BUB-1 recruits PP2A:B56 to the chromosomes via dual mechanism: 1) PPTR-1/2 interacts with the newly identified LxxIxE short linear motif (SLiM) within a disordered region in BUB-1 in a phosphorylation-dependent manner; and 2) PPTR-2 can also be recruited to chromosomes in a BUB-1 kinase domain-dependent manner. Our results highlight a novel, BUB-1-dependent mechanism for B56 recruitment, essential for recruiting a pool of PP2A required for proper chromosome congression during meiosis I.

23 **INTRODUCTION**

24 Formation of a diploid embryo requires that sperm and egg contribute exactly one copy of
25 each chromosome. The cell division in charge of reducing ploidy of the genome is meiosis,
26 which involves two chromosome segregation steps after a single round of DNA replication
27 (Marston and Amon, 2004; Ohkura, 2015). Female meiosis is particularly error-prone
28 (Hassold and Hunt, 2001) which can lead to chromosomally abnormal embryos. Therefore,
29 understanding the molecular events that guarantee proper chromosome segregation during
30 female meiosis is of paramount importance. Cell division is under tight control of post-
31 translational modifications (PTMs), of which phosphorylation is the most studied. The
32 balance between kinase and phosphatase activities play a central role but we still lack a clear
33 picture of how this is achieved during meiosis, especially when compared to mitosis (Gelens
34 et al., 2018; Novak et al., 2010).

35

36 Protein Phosphatase 2A (PP2A) is a heterotrimeric serine/threonine phosphatase composed of
37 a catalytic subunit C (PPP2C), a scaffolding subunit A (PPP2R1) and a regulatory subunit B
38 (PPP2R2-PPP2R5) (Cho and Xu, 2007; Xu et al., 2008; Xu et al., 2006). While the core
39 enzyme (A and C subunits) is invariant, diversity in PP2A holoenzyme composition arises
40 from the different regulatory B subunits. Four families of B subunits have been characterised:
41 B55 (B), B56 (B′), PR72 (B″), and Striatin (B‴) (Moura and Conde, 2019; Seshacharyulu et
42 al., 2013; Shi, 2009). In mammals and yeast, PP2A:B56 regulates the spindle assembly
43 checkpoint (SAC) (Espert et al., 2014; Hayward et al., 2019; Qian et al., 2017; Vallardi et al.,
44 2019), chromosome congression (Xu et al., 2013; Xu et al., 2014), and centromeric cohesion
45 (Kitajima et al., 2006; Riedel et al., 2006; Tang et al., 2006).

46

47 PP2A:B56 can be targeted to distinct sites by different proteins and two mechanisms have
48 been characterised at the structural level. While an N-terminal coiled coil domain in
49 Shugoshin/MEI-S332 binds PP2A:B56 (Xu et al., 2009), other substrates and/or regulatory
50 proteins contain short linear motifs (SLiMs) following the consensus LxxIxE, which interact
51 directly with B56 subunits (Hertz et al., 2016; Van Roey and Davey, 2015; Wang et al.,
52 2016). BubR1 is one of the most widely studied LxxIxE-containing proteins, and has been
53 well characterised during mitosis, where it plays a role in targeting PP2A:B56 to kinetochores
54 (Foley et al., 2011; Kruse et al., 2013; Suijkerbuijk et al., 2012). BubR1 is also required
55 during mouse meiosis (Homer et al., 2009; Touati et al., 2015; Yoshida et al., 2015) where
56 kinetochore-microtubule attachments are stabilized through kinetochore dephosphorylation by
57 PP2A:B56 (Yoshida et al., 2015).
58
59 In *C. elegans*, the meiotic role of PP2A remains unexplored. The core components of the
60 PP2A holoenzyme in *C. elegans* are LET-92 (catalytic C subunit) and PAA-1 (scaffolding A
61 subunit), and the regulatory B subunits are $B55^{SUR-6}$ (Sieburth et al., 1999), $B56^{PPTR-1}$ and
62 $B56^{PPTR-2}$ (Padmanabhan et al., 2009), $B72^{RSA-1}$ (Schlaitz et al., 2007), and CASH-1/Striatin
63 (Pal et al., 2017). PP2A complexes containing $B55^{SUR-6}$ and $B72^{RSA-1}$ play important roles
64 during mitosis (Kitagawa et al., 2011; Schlaitz et al., 2007; Song et al., 2011), and, while
65 PP2A likely plays a role during meiosis (Schlaitz et al., 2007), this has not been studied.
66 Interestingly, the closest *C. elegans* BubR1 orthologue $Mad3^{SAN-1}$, does not localise to
67 unattached kinetochores (Essex et al., 2009) and lacks the domain responsible for PP2A:B56
68 targeting. Additionally, the *C. elegans* Shugoshin orthologue, SGO-1, is dispensable for
69 protection of cohesion in meiosis I (de Carvalho et al., 2008) and for counteracting Aurora B-
70 targeting histone H3T3 phosphorylation (Ferrandiz et al., 2018). These observations suggest
71 the existence of additional unknown mechanisms of PP2A regulation.

72 In the present work, we used *C. elegans* oocytes to establish the role and regulation of PP2A
73 during female meiosis. We found that PP2A is essential for female meiosis and its recruitment
74 to meiotic chromosomes and spindle is mediated by the B56 regulatory subunits PPTR-1 and
75 PPTR-2. Targeting of the B56 subunits is mediated by the kinase BUB-1 through a canonical
76 B56 LxxIxE motif which targets both PPTR-1 and PPTR-2 to the chromosomes and central-
77 spindle during meiosis. Overall, we provide evidence for a novel, BUB-1-regulated role for
78 PP2A:B56 in chromosome congression during female meiosis.

79 **RESULTS**

80 **Protein Phosphatase 2A is essential for spindle assembly and chromosome segregation**
81 **during meiosis I**

82 We used dissected *C. elegans* oocytes to assess the role and regulation of PP2A (see Figure
83 1A for schematic) during female meiosis by following spindle and chromosome dynamics
84 using GFP-tagged tubulin and mCherry-tagged histone. During meiosis I, six pairs of
85 homologous chromosomes (bivalents) are captured by an acentrosomal spindle.
86 Chromosomes then align and segregate. For our analysis, we defined Metaphase I (t = 0) as
87 the frame before we detected chromosome separation (Figure 1B). In wild type oocytes,
88 chromosome segregation is associated with dramatic changes in microtubule organisation as
89 anaphase progresses, with microtubule density decreasing in poles and the bulk of
90 GFP::tubulin is detected in the central-spindle (Figure 1C; Supp. Movie 1). In contrast,
91 depletion of the PP2A catalytic subunit LET-92 drastically affects meiosis I with
92 chromosomes failing to align in 84% of the oocytes (Figure 1C, cyan arrow; Figure 1D;
93 P<0.0001, Fisher's exact test). During anaphase, chromosomes collapse into a small area
94 where, in some cases, two chromosome masses were visible (Figure 1C, yellow arrow).
95 Interestingly, severe chromosome segregation defects do not necessarily lead to polar body
96 extrusion (PBE) defects (Schlientz and Bowerman, 2020). In the absence of PP2Ac only 15%
97 of oocytes achieved polar body extrusion (Figure 1E, P<0.0001, Fisher's exact test). Similar
98 defects were observed by depleting the sole PP2A scaffolding subunit, PAA-1 (Figure S1A-
99 C). In *let-92(RNAi)* and *paa-1(RNAi)* oocytes microtubules do not organise into a bipolar
100 structure (Figure 1B and Figure S1A, magenta arrows), as assessed by localisation of the
101 spindle pole protein GFP::ASPM-1 (Connolly et al., 2014). GFP::ASPM-1 displays two
102 focused poles in 100% of wild type oocytes (Figure 1F,G, cyan arrows). In contrast,

103 GFP::ASPM-1 foci fail to coalesce in 95% of *let-92(RNAi)* oocytes, displaying a cluster of
104 small foci (Figure 1F, orange arrows; Figure 1G; Supp. Movie 2).
105 We then sought to determine whether the lack of chromosome segregation was due to a defect
106 in meiosis I progression. We measured endogenously GFP-tagged Securin^{IFY-1} levels as a
107 readout for Anaphase Promoting Complex/Cyclosome (APC/C) activity (i.e. anaphase
108 progression). Cytoplasmic Securin^{IFY-1} degradation proceeded at similar rates in wild type and
109 LET-92-depleted oocytes (Figure 1H,I; Supp. Movie 3), indicating that APC/C activity is
110 largely unperturbed in the absence of PP2A. Given the similarity of this phenotype to the
111 depletion of CLASP orthologue CLS-2 I (Dumont et al., 2010; Laband et al., 2017; Schlientz
112 and Bowerman, 2020), we analysed the localisation of CLS-2 and detected no changes in
113 CLS-2 levels throughout meiosis (Figure S2; Supp Movie 4).
114 Taken together, we have found that PP2A is required for spindle assembly, chromosome
115 alignment, and polar body extrusion during meiosis I. Additionally, APC activity is
116 unperturbed by PP2A depletion, but we cannot rule out an impact on other pathways acting
117 redundantly with APC (Sonneville and Gonczy, 2004; Wang et al., 2013).
118

119 **PP2A:B56 localises to meiotic chromosomes and spindle**

120 To assess the localisation of the core PP2A enzyme (A and C subunits) in vivo we attempted
121 to tag endogenous LET-92 with GFP but were unsuccessful, presumably due to disruption of
122 its native structure, in agreement with a recent report (Magescas et al., 2019). We generated a
123 GFP-tagged version of the sole *C. elegans* PP2A scaffold subunit, PAA-1, and used this to
124 assess the localisation of the core enzyme during meiosis I (Figure 2A; Supp Movie 5). The
125 fusion protein localised in centrosomes and P-granules during the early embryonic mitotic
126 divisions (Figure S3A), in agreement with previous immunofluorescence data (Lange et al.,
127 2013). During meiosis I, GFP::PAA-1 localises to spindle poles (Figure 2A, cyan arrows) and

128 chromosomes (Figure 2A, magenta arrows). The chromosomal signal is a combination of
129 midbivalent and kinetochore populations, visible when analysing single Z-planes in the time-
130 lapses (Figure S3B, magenta and yellow arrows). As meiosis I progresses, GFP::PAA-1
131 signal concentrates in the central-spindle between the segregating chromosomes (Figure 2A,
132 magenta arrowhead), finally disappearing by late anaphase I. This pattern differs substantially
133 from that of Protein Phosphatase 1 (PP1) which localises in the characteristic cup-shaped
134 kinetochores (Hattersley et al., 2016).
135
136 To address which regulatory subunits are involved in targeting PP2A to the meiotic spindle
137 and chromosomes, we first assessed the localisation of the two *C. elegans* B56 orthologues,
138 PPTR-1 and PPTR-2 and the single B55 orthologue, SUR-6 (Figure S4A). Live imaging of
139 endogenous, GFP-tagged regulatory subunits revealed that both B56 orthologues, PPTR-1 and
140 PPTR-2, localised strongly and dynamically within the meiotic spindle whereas no spindle or
141 chromosome localisation of $B55^{SUR-6}$ could be detected (Figure S4B). PPTR-1 has the highest
142 sequence identity with human B56α2 (68.3%) and ε3 (71.87%) whereas PPTR-2 displays the
143 highest sequence identity with human B56δ3 (66.19%) and B56γ1 (68.97%) (Table 1 and
144 Supp. Table 1). Closer analysis of the C-terminal sequence in B56 which plays a key role in
145 specifying centromere versus kinetochore localisation (Vallardi et al., 2019), further
146 confirmed that PPTR-1 displays the highest sequence identity with the centromeric B56s,
147 α and ε (93.75% and 87.5% respectively), while PPTR-2 displays the highest sequence
148 identity with the kinetochore-localised B56, γ and δ (93.75% and 100%) (Figure S4C). We
149 will henceforth refer to PPTR-1 as $B56\alpha^{PPTR-1}$ and to PPTR-2 as $B56\gamma^{PPTR-2}$. We used
150 endogenous GFP-tagged versions of $B56\alpha^{PPTR-1}$ and $B56\gamma^{PPTR-2}$ (Kim et al., 2017) and
151 analysed their dynamic localisation pattern in greater spatial and temporal detail. $B56\alpha^{PPTR-1}$
152 localises mainly to the region between homologous chromosomes (midbivalent) during

153 metaphase of meiosis I (Figure 2B, magenta arrow; Supp. Movie 6) and faintly in
154 kinetochores (Figure 2B, yellow arrows). During anaphase I, B56α^{PPTR-1} is present
155 exclusively on the central spindle (Figure 2B, magenta arrowhead; Supp. Movie 6). B56γ^{PPTR-}
156 ^{2} localises mainly in the midbivalent during metaphase of meiosis I (Figure 2C, magenta
157 arrow; Supp. Movie 7) and faintly in kinetochores (Figure 2C, yellow arrow). A difference
158 between the two paralogs arises during anaphase: B56γ^{PPTR2} is present in the central spindle
159 and on chromosomes (Figure 2C, magenta and yellow arrowheads; Supp. Movie 7). In spite
160 of this difference, the levels of B56α^{PPTR-1} and B56γ^{PPTR-2} within the meiotic spindle follow
161 similar dynamics (Figure S5A-C).
162 These results show that *C. elegans* B56 subunits, like their mammalian counterparts, display a
163 similar but not identical localisation pattern: while both B56α^{PPTR-1} and B56γ^{PPTR-2} are present
164 in the midbivalent and central spindle, B56γ^{PPTR-2} is also associated with chromosomes during
165 anaphase.
166
167 **Depletion of B56α^{PPTR-1} and B56γ^{PPTR-2} leads to chromosome congression defects**
168 To address the role of the *C. elegans* B56 subunits during meiosis I, we combined a B56γ^{PPTR-}
169 ^{2} deletion allele (*ok1467*, '*pptr-2Δ*') with RNAi-mediated depletion of B56α^{PPTR-1} ('*pptr-*
170 *1(RNAi)*'), which we will refer to hereafter as 'PPTR-1/2 depletion'. While there was no
171 significant change in GFP::PAA-1 localisation upon depletion of B56α^{PPTR-1} or deletion of
172 B56γ^{PPTR-2}, no PAA-1 signal is detected associated with chromosomes upon double PPTR-1/2
173 depletion (Figure 2D, magenta arrow; Supp. Movie 8). Of note, PP2A targeting to poles was
174 still detected (Figure 2D, cyan arrows), indicating that B56 subunits target PP2A complex to
175 chromosomes but are not necessary for spindle pole targeting (Figure 2D; Supp. Movie 8).
176 We noticed that chromosomes failed to align upon PPTR-1/2 depletion (Figure 2D, yellow
177 arrow) and in order to quantify this phenotype, we measured the angle between the bivalent

178 long axis and the spindle axis ('θ', Figure 2F, Figure S6) and the distance between the centre
179 of the midbivalent and the metaphase plate, defined as the line in the middle of the spindle
180 ('d', Figure 2G, Figure S6). We chose a time of 80 seconds prior to metaphase I for the
181 analysis since most chromosomes are aligned by this stage (Figure S6) in agreement with
182 previous data (Hattersley et al., 2016). Both the angle (θ) and the distance (d) increased
183 significantly upon PPTR-1/2 double depletion (Figure 2F,G).Taken together, these results
184 indicate that B56 subunits are involved in chromosomal and central spindle targeting PP2A
185 and play a role in chromosome congression prior to anaphase. The PAA-1 localisation and
186 chromosome alignment defects observed upon PPTR-1/2 depletion suggest that the subunits
187 are at least partially redundant.
188
189 **Shugoshin^{SGO-1} and BUBR1/Mad3^{SAN-1} are not essential for B56 subunit targeting**
190 We next sought to identify the protein(s) involved in targeting PP2A:B56 to meiotic
191 chromosomes. Two of the most studied proteins involved in B56 targeting are Shugoshin and
192 BubR1. The BubR1 orthologue, Mad3^{SAN-1} is not detected in meiotic chromosomes or spindle
193 (Figure S7A) and Mad3^{SAN-1} depletion by RNAi or a Mad3^{SAN-1} deletion allele (*ok1580*) does
194 not inhibit B56 localisation (Figure S7B,C). We therefore tested the role of the Shugoshin
195 ortholog, SGO-1. We used a *sgo-1* deletion allele generated by CRISPR (Ferrandiz et al.,
196 2018; Figure S7A) and observed no change in B56α^{PPTR-1} levels (Figure S8B,C) and a slight
197 reduction in B56γ^{PPTR-2} levels (Figure S8D,E). The PPTR-2 signal decreased between 20-
198 40% in the *sgo-1Δ* mutant (Figure S8E, shaded area) and this reduction correlated with the
199 timing of the congression defect in XX depletion (prior to metaphase I). Hence, Mad3^{SAN-1}
200 and Shugoshin^{SGO-1} are not essential in PP2A:B56 targeting during meiosis in *C. elegans*
201 oocytes.
202

203 **BUB-1 targets B56 subunits through a conserved LxxIxE motif**

204 *C. elegans* B56 subunits display a dynamic localisation pattern similar to that of the kinase
205 BUB-1 throughout meiosis I (Dumont et al., 2010; Monen et al., 2005; Pelisch et al., 2019;
206 Pelisch et al., 2017) and interestingly, BUB-1 depletion by RNAi or using an auxin-inducible
207 degradation system leads to alignment and segregation defects during meiosis (Dumont et al.,
208 2010; Pelisch et al., 2019). We therefore tested whether BUB-1 is involved in B56 subunits
209 recruitment to meiotic chromosomes. RNAi-mediated depletion of BUB-1 abolished meiotic
210 chromosome localisation of B56α^{PPTR-1} (Figure 3A,B; Supp. Movie 9) and B56γ^{PPTR-2} (Figure
211 3C,D; Supp. Movie 10). GFP::PAA-1 localisation on chromosomes was also abolished by
212 BUB-1 depletion (Figure 3E; Supp Movie 11). While we could not address the intensity on
213 spindle poles due to the strong spindle defect in the absence of BUB-1, we could detect
214 GFP::PAA-1 in extrachromosomal regions (Figure 3E, cyan arrows), indicating that BUB-1
215 specifically regulates PP2A:B56 chromosomal targeting. Consistent with this idea, BUB-1
216 depletion does not affect the localisation of the catalytic subunit of another major
217 phosphatase, PP1^{GSP-2} (Figure S9; Supp. Movie 12). In agreement with published data
218 (Dumont et al., 2010), BUB-1 depletion causes severe defects in chromosome alignment
219 (Figure 3F).

220 *C. elegans* BUB-1 contains a conserved N-terminal tetratricopeptide repeat (TPR) domain, a
221 C-terminal kinase domain, and regions mediating its interaction with Cdc20 and BUB3
222 (ABBA and GLEBS motifs, respectively) (Figure 4A; Kim et al., 2017; Kim et al., 2015;
223 Moyle et al., 2014). Sequence analysis of *C. elegans* BUB-1 revealed the presence of a
224 putative B56 LxxIxE motif in residues 282-287 (Figure 4A). When compared with two well-
225 characterised LxxIxE motifs, in BubR1 and RepoMan, there is a high degree of conservation
226 in the key residues making contacts with the B56 hydrophobic pockets (Figure 4A). In
227 addition, the SLiM-binding hydrophobic pocket in B56 subunits is very well conserved in *C.*

228 *elegans* (Figure S10). The putative LxxIxE motif lies within a region predicted to be
229 disordered (Figure 4B) with serine 283 fitting a Cdk1 Ser/Thr-Pro motif.
230 Using a fluorescence polarisation-based assay, we confirmed that the LxxIxE motif of BUB-1
231 binds to purified recombinant PPTR-2, and this binding is abolished by the L282A,V285A
232 mutations (Figure 4C). While localisation of BUB-1^{L282A,V285A} was indistinguishable from
233 that of wild type BUB-1 during metaphase I (Figure S11A), localisation of B56α^{PPTR-1} to the
234 midbivalent and central spindle was almost completely lost in the BUB-1^{L282A,V285A} mutant
235 (Figure 4D-F; Supp. Movie 13). B56γ^{PPTR-2} midbivalent localisation leading to metaphase I
236 and central-spindle localisation during anaphase were also dependent on the BUB-1 LxxIxE
237 motif (Figure 4G, magenta arrows, and 4H; Supp. Movie 14). In contrast, chromosome-
238 associated B56γ^{PPTR-2} was less affected in the BUB-1^{L282A,V285A} mutant (Figure 4G, yellow
239 arrows). Importantly, the LxxIxE motif mutations BUB-1^{L282A,V285A} abrogates GFP::PAA-1
240 localisation in the midbivalent and central spindle (Figure 4I, magenta arrows; Supp Movie
241 15) without affecting the spindle pole PAA-1 localisation (Figure 4I, cyan arrows; Supp
242 Movie 15). Some GFP::PAA-1 signal was still detected in anaphase chromosomes, consistent
243 with the remaining B56γ^{PPTR-2} on chromosomes (Figure 4I,J, yellow arrows). This LxxIxE
244 motif-dependent regulation is specific for B56 subunits because the localisation of the spindle
245 assembly checkpoint component Mad1^{MDF-1}, a known BUB-1 interactor (Moyle et al., 2014),
246 is not disrupted after mutating the BUB-1 LxxIxE motif (Figure S11B). Mutation of the BUB-
247 1 LxxIxE motif not only impairs B56 chromosomal targeting but also leads to
248 alignment/congression defects (Figure 4K,L), indicating that the BUB-1 LxxIxE motif
249 recruits PP2A:B56 and plays an important role in chromosome congression. Lagging
250 chromosomes were detected in 36% of oocytes in the BUB-1^{L282A,V285A} mutant, versus 10% in
251 wild type oocytes (P=0.0125, Fisher's exact test), but segregation was achieved in 100% of
252 the cases with no polar body extrusion defects were detected. Interestingly, the newly

253 identified LxxIxE motif specifically recruits PP2A:B56 to metaphase chromosomes and
254 anaphase central spindle, but not anaphase chromosomes.
255
256 **Phosphorylation of BUB-1 LxxIxE is important for PP2A:B56 chromosome targeting**
257 Since phosphorylation of LxxIxE motifs can increase affinity for B56 by ~10-fold (Wang et
258 al., 2016), we sought to determine if Ser 283 within BUB-1 LxxIxE motif is phosphorylated
259 in vivo. To this end, we immunoprecipitated endogenous, GFP-tagged BUB-1 from embryo
260 lysates using a GFP nanobody. Immunoprecipitated material was digested with trypsin,
261 peptides analysed by mass spectrometry and searches conducted for peptides containing
262 phosphorylated adducts. As expected GFP-tagged, but not untagged, BUB-1 was pulled down
263 by the GFP nanobody (Figure S12A) along with the BUB-1 partner, BUB-3 (Figure 5A, blue
264 arrow). We found four phospho-sites clustered within a disordered region, one of which is Ser
265 283, within the LxxIxE motif (Figure 5B; see also representative MS spectra for Ser 283 in
266 Figure S12B). We expressed a BUB-1 fragment containing the LxxIxE motif (Figure 5C) and
267 performed Cdk1 kinase assays, which showed that Cdk1 can phosphorylate the 259-332
268 BUB-1 fragment (Figure 5D). Western blot analysis using a phospho-specific antibody
269 revealed that Cdk1 can phosphorylate Ser 283 in vitro (Figure 5E). Importantly, LxxIxE motif
270 peptides with phosphorylated Ser 283 bound recombinant B56γ^{PPTR-2} with higher affinity than
271 non-phosphorylated LxxIxE peptide (Figure 5F). During meiosis, while BUB-1
272 phosphorylated in Ser 283 is detected in midbivalent and kinetochore, it is preferentially
273 enriched in the midbivalent (Figure 5G,H).
274 Mutating the Ser 283 to Ala in endogenous BUB-1 ('BUB-1^{S283A}') had a similar effect to that
275 of the BUB-1^{L282A,V285A} mutant: it significantly reduced B56α^{PPTR-1} localisation (Figure 6A,B;
276 Supp. Movie S16) and in the case of B56γ^{PPTR-2}, it significantly reduced its midbivalent and
277 central spindle localisation (Figure 6C,D; Supp. Movie S17). In line with these results and

278 consistent with a B56-dependent chromatin recruitment of PP2A, GFP::PAA-1 was not
279 detected on chromosomes during prometaphase/metaphase in the BUB-1^{S283A} mutant (Figure
280 6E,F; Supp. Movie S18). BUB-1^{S283A} mutation not only impairs PP2A/B56 chromosomal
281 targeting but also leads to alignment/congression defects (Figure 6G,H), indicating that
282 phosphorylation of Ser 283 within the BUB-1 LxxIxE motif recruits PP2A/B56 and plays an
283 important role in chromosome congression.

284 **Anaphase chromosomal recruitment of PP2A:B56γ^{PPTR-2} depends on BUB-1 C-terminal**
285 **kinase domain**

286 Since not all of B56γ^{PPTR-2} is targeted by the BUB-1 LxxIxE motif, we turned our attention to
287 BUB-1 kinase domain. In *C. elegans* BUB-1 kinase domain regulates its interaction with
288 binding partners such as Mad1^{MDF-1}. The K718R/D847N double mutation (equivalent to
289 positions K821 and D917 in human Bub1) destabilizes the kinase domain and prevents its
290 interaction with Mad1^{MDF-1} (Moyle et al., 2014). We generated endogenous BUB-1^{K718R,D847N}
291 (Figure 7A) and confirmed that these mutations abolish recruitment of Mad1^{MDF-1} (Figure
292 S11B). B56α^{PPTR-1}::GFP localisation and dynamics remained largely unaltered in the mutant
293 BUB-1^{K718R,D847N} (Figure S13; Supp. Movie 19). The B56γ^{PPTR-2}::GFP pool most affected by
294 the K718R,D847N mutant was the chromosomal one (Figure 7B, yellow arrows; Supp. Movie
295 20) with the central-spindle pool reduced but still present (Figure 7B, magenta arrow; Supp.
296 Movie 20). We therefore combined the K718R,D847N with the L282A,V285A mutations to
297 generate 'BUB-1 $^{L282A,V285A;K718R,D847N}$' observed a significant decrease in both chromosomal
298 and central spindle B56γ^{PPTR-2}::GFP (Figure 7B; Supp. Movie 20). Line profiles highlighting
299 these localisation differences in the mutants are shown in Figure 7C. We then analysed
300 GFP::PAA-1 was not found associated with chromosomes during prometaphase I in the BUB-
301 1$^{L282A,V285A;K718R,D847N}$ mutant (Figure 7E, magenta arrow; Supp. Movie 21). Of note, a

302 significant population of GFP::PAA-1 remained associated with spindles poles (Figure 7D,
303 cyan arrows) and surrounding the spindle area during anaphase (Figure 7D, yellow arrows).
304 These results show that the BUB-1 kinase domain is important for recruitment of B56γ^{PPTR-2}
305 but not of B56α^{PPTR-1}. Thus, BUB-1 is a key factor for the recruitment of PP2A:B56 but could
306 also provide the basis for establishing (probably together with other proteins) the two pools of
307 B56γ^{PPTR-2}.

308 **DISCUSSION**

309 In the present manuscript, we have uncovered new roles for PP2A during oocyte meiosis in *C.*
310 *elegans.* PP2A is essential for meiosis I: depletion of the catalytic or scaffold subunits lead to
311 severe spindle assembly defects, lack of chromosome segregation, and failure to achieve polar
312 body extrusion. These effects are a likely brought about by a combination of different PP2A
313 subcomplexes with varying regulatory B subunits. PP2A:B56 regulates chromosome
314 dynamics prior to segregation, since depletion of the two B56 orthologues, PPTR-1 and
315 PPTR-2 lead to alignment defects. We have uncovered a new phospho-regulated B56 LxxIxE
316 motif in *C. elegans* BUB-1 that recruits PP2A:B56 and is important for chromosome
317 alignment during meiosis I.

318

319 **Dissecting the role of PP2A during oocyte meiosis**

320 Depletion of the sole catalytic or scaffold PP2A subunits lead to massive meiotic failure and
321 embryonic lethality. The earliest effect we could see in our experimental setup is a failure to
322 assemble a bipolar spindle. This will of course have a direct impact on any process that
323 should occur after spindle assembly, including chromosome alignment and segregation,
324 followed by polar body extrusion. However, BUB-1 depletion leads to a severe spindle
325 assembly defect, followed by alignment defects. Then, in the majority of cases chromosomes
326 segregate (with visible errors – lagging chromosomes) and polar bodies do extrude. Hence,
327 lack of a proper bipolar metaphase spindle is not sufficient to result in lack of segregation or
328 polar body extrusion. Along this line, PP2A complexes harbouring the B56 subunits PPTR-1
329 and PPTR-2 are important to target the phosphatase to chromosomes to regulate chromosome
330 alignment in metaphase I. Furthermore, this chromosomal B56 pool is recruited by BUB-1
331 through its LxxIxE SLiM motif. Mutation of this motif that abolish binding to B56 subunits
332 leads to alignment defects. B56 subunits however are not involved in spindle pole targeting of

333 PP2A, suggesting that it is this spindle pole pool the one relevant for spindle assembly. Our
334 attempts to address a possible role for other B subunits where focused on RSA-1 and SUR-6
335 given their reported centrosomal roles during mitosis (Enos et al., 2018; Kitagawa et al.,
336 2011; Schlaitz et al., 2007; Song et al., 2011). However, neither RSA-1 nor SUR-6 were
337 required for meiotic spindle assembly. It is likely that the role of PP2A on spindle assembly is
338 achieved by a combination of B subunits and that could also include uncharacterised B
339 subunits (Bye-A-Jee et al., 2020).
340

341 **B56 targeting during different stages of meiosis I**

342 Chromosomal PPTR-1 and PPTR-2 and the ensuing PP2A targeting prior to chromosome
343 segregation depends on the BUB-1 LxxIxE motif. Interestingly, this dependency changes
344 during anaphase, where PPTR-2 chromosomal targeting is BUB-1-dependent but LxxIxE
345 motif-independent and depends on the kinase domain. The regulation of protein localisation
346 during meiosis I in *C. elegans* oocytes is highly dynamic and differences have been observed
347 between metaphase and anaphase. For example, while kinetochore localisation of the CLASP
348 orthologue CLS-2 during metaphase depends on BUB-1, a pool of CLS-2 is able localise in
349 the anaphase central spindle in a BUB-1-independent manner (Laband et al., 2017). In this
350 line, since its role during meiosis was first described (Dumont et al., 2010), there has been no
351 clear explanation as to the cause of the alignment and segregation defects upon BUB-1
352 depletion. Our results provide a plausible explanation for the role of BUB-1 in chromosome
353 alignment during oocyte meiosis in *C. elegans* through the recruitment of PP2A/B56.
354

355 **Possible function of chromosome-associated PP2A**

356 As mentioned above, the PP2A complexes are likely playing a number of important roles
357 during meiosis. Our work uncovers a function during chromosome congression involving

358 B56 subunits targeted by BUB-1. Similar to mice and yeast, it is therefore likely that PP2A
359 complexes at the chromosome control proper chromosome-spindle attachments. The
360 alignment defects we observed upon PPTR-1/2 depletion (or in the LxxIxE motif mutant)
361 resemble those reported in the absence of kinetochore proteins (Danlasky et al., 2020;
362 Dumont et al., 2010). Interestingly, PP2A:B56 complexes containing PPTR-1 and PPTR-2
363 are present at the meiotic kinetochore, and it is therefore possible that PP2A/B56 works in
364 parallel to and/or regulates kinetochore protein(s). Furthermore, we detected GFP::PAA-1 on
365 anaphase chromosomes, similar to kinetochore proteins (Danlasky et al., 2020; Dumont et
366 al., 2010; Hattersley et al., 2016).
367
368 During meiosis in *C. elegans*, the Aurora B orthologue, AIR-2, concentrates in the interface
369 between homologous chromosomes (i.e. the midbivalent (Kaitna et al., 2002; Rogers et al.,
370 2002; Schumacher et al., 1998) and its activity is counteracted by PP1, which is recruited by
371 the protein LAB-1 (Tzur et al., 2012). PP1 counteracts Aurora B^{AIR-2} during meiosis by
372 antagonising Haspin-mediated H3T3 phosphorylation in the long arm of the bivalent
373 (Ferrandiz et al., 2018). Consistent with this, PP1 depletion leads to loss of sister chromatid
374 cohesion during meiosis I (Kaitna et al., 2002; Rogers et al., 2002). During prometaphase
375 and metaphase I, Aurora B^{AIR-2} is retained in the bivalent whereas PP1 resides mainly in
376 kinetochores (Hattersley et al., 2016) and it is therefore likely that another phosphatase(s)
377 will be involved in controlling Aurora B-mediated phosphorylation events during metaphase
378 I. Since PP2A:B56 is concentrated in the midbivalent during meiosis I, we hypothesise that it
379 could be the phosphatase balancing AIR-2 activity during meiosis. In this respect, we found
380 that serine 612 in BUB-1 is phosphorylated and this serine is embedded in a sequence
381 (RRL<u>S</u>I) closely resembling the consensus for PP2A:B56 reported in (Kruse et al., 2020).
382 Furthermore, the sequence also fits into the loosely defined Aurora B consensus RRxSφ

383 (where φ is a hydrophobic aa) (Cheeseman et al., 2002; Deretic et al., 2019; Kettenbach et
384 al., 2011). Therefore, BUB-1 itself could be subject to an Aurora B-PP2A:B56 balance and it
385 will be very interesting to address if BUB-1 and other meiotic proteins are regulated by the
386 balance between Aurora B and PP2A:B56.
387
388 In summary, we provide evidence for a novel, BUB-1-regulated role for PP2A:B56 during
389 female meiosis in *C. elegans.* It will be interesting to test in the future our hypothesis that
390 PP2A is the main phosphatase counteracting Aurora B-mediated phosphorylation to achieve
391 proper phosphorylation levels during meiosis I.
392

ACKNOWLEDGEMENTS

We would like to thank Guy Benian, Needhi Bhalla, Bruce Bowerman, Arshad Desai, Tony Hyman, and Enrique Martinez-Perez for sharing *C. elegans* strains and antibodies. We would like to thank Egon Ogris for sharing unpublished data on the use of the PP2Ac monoclonal antibody. We thank Arshad Desai, Ron Hay, and Tomo Tanaka for comments on the manuscript. This work was supported by a Career Development Award from the Medical Research Council (grant MR/R008574/1) and an ISSF grant funded by the Wellcome Trust (105606/Z/14/Z). ST is funded by a Medical Research Council Doctoral Training Programme. D.K.C. is supported by a Sir Henry Dale Fellowship from the Wellcome Trust (208833). P.L-G. and J.B. were supported by NIH grant R01 GM074215, awarded to Arshad Desai. Work in the J.N.B. lab is supported by NIH grant R01 GM114471. We acknowledge the FingerPrints Proteomics Facility and the Dundee Imaging Facility, which are supported by a 'Wellcome Trust Technology Platform' award (097945/B/11/Z) and the Tissue Imaging Facility, funded by a Wellcome Trust award (101468/Z/13/Z). Some nematode strains were provided by the CGC, which is funded by NIH Office of Research Infrastructure Programs (P40 OD010440).

AUTHOR CONTRIBUTIONS

L.B B. Investigation; formal analysis; writing – review and editing.

F.S. Investigation; Formal analysis; writing – review and editing.

S.J.P.T. Investigation; writing – review and editing.

C.F B. Investigation; writing – review and editing.

J.B. Investigation.

P.L-G. Investigation; writing – review and editing.

C.G.S.T. Investigation; writing – review and editing.

J.N.B. Investigation; writing – review and editing.

D.K.C. Investigation; writing – review and editing.

F.P. Funding acquisition; conceptualisation; project administration; investigation; methodology; supervision; formal analysis. writing – original draft. writing – review and editing.

421 **REFERENCES**

422 Allan, C., Burel, J.M., Moore, J., Blackburn, C., Linkert, M., Loynton, S., Macdonald, D.,
423 Moore, W.J., Neves, C., Patterson, A.*, et al.* (2012). OMERO: flexible, model-driven data
424 management for experimental biology. Nat Methods *9*, 245-253.
425 Bye-A-Jee, H., Zaru, R., Magrane, M., Orchard, S., and Consortium, t.U. (2020).
426 Caenorhabditis elegans phosphatase complexes in UniProtKB and Complex Portal. The FEBS
427 Journal *287*, 2664-2684.
428 Cheeseman, I.M., Anderson, S., Jwa, M., Green, E.M., Kang, J., Yates, J.R., 3rd, Chan, C.S.,
429 Drubin, D.G., and Barnes, G. (2002). Phospho-regulation of kinetochore-microtubule
430 attachments by the Aurora kinase Ipl1p. Cell *111*, 163-172.
431 Cho, U.S., and Xu, W. (2007). Crystal structure of a protein phosphatase 2A heterotrimeric
432 holoenzyme. Nature *445*, 53-57.
433 Connolly, A.A., Osterberg, V., Christensen, S., Price, M., Lu, C., Chicas-Cruz, K., Lockery,
434 S., Mains, P.E., and Bowerman, B. (2014). Caenorhabditis elegans oocyte meiotic spindle
435 pole assembly requires microtubule severing and the calponin homology domain protein
436 ASPM-1. Mol Biol Cell *25*, 1298-1311.
437 Danlasky, B.M., Panzica, M.T., McNally, K.P., Vargas, E., Bailey, C., Li, W., Gong, T.,
438 Fishman, E.S., Jiang, X., and McNally, F.J. (2020). Evidence for anaphase pulling forces
439 during C. elegans meiosis. J Cell Biol *219*.
440 de Carvalho, C.E., Zaaijer, S., Smolikov, S., Gu, Y., Schumacher, J.M., and Colaiacovo, M.P.
441 (2008). LAB-1 antagonizes the Aurora B kinase in C. elegans. Genes Dev *22*, 2869-2885.
442 Deretic, J., Kerr, A., and Welburn, J.P.I. (2019). A rapid computational approach identifies
443 SPICE1 as an Aurora kinase substrate. Mol Biol Cell *30*, 312-323.

444 Desai, A., Rybina, S., Müller-Reichert, T., Shevchenko, A., Shevchenko, A., Hyman, A., and
445 Oegema, K. (2003). KNL-1 directs assembly of the microtubule-binding interface of the
446 kinetochore in C. elegans. Genes & Development *17*, 2421-2435.
447 Dickinson, D.J., Pani, A.M., Heppert, J.K., Higgins, C.D., and Goldstein, B. (2015).
448 Streamlined Genome Engineering with a Self-Excising Drug Selection Cassette. Genetics
449 *200*, 1035-1049.
450 Dumont, J., Oegema, K., and Desai, A. (2010). A kinetochore-independent mechanism drives
451 anaphase chromosome separation during acentrosomal meiosis. Nat Cell Biol *12*, 894-901.
452 Enos, S.J., Dressler, M., Gomes, B.F., Hyman, A.A., and Woodruff, J.B. (2018). Phosphatase
453 PP2A and microtubule-mediated pulling forces disassemble centrosomes during mitotic exit.
454 Biology Open *7*, bio029777.
455 Espert, A., Uluocak, P., Bastos, R.N., Mangat, D., Graab, P., and Gruneberg, U. (2014).
456 PP2A-B56 opposes Mps1 phosphorylation of Knl1 and thereby promotes spindle assembly
457 checkpoint silencing. The Journal of Cell Biology *206*, 833.
458 Essex, A., Dammermann, A., Lewellyn, L., Oegema, K., and Desai, A. (2009). Systematic
459 analysis in Caenorhabditis elegans reveals that the spindle checkpoint is composed of two
460 largely independent branches. Mol Biol Cell *20*, 1252-1267.
461 Ferrandiz, N., Barroso, C., Telecan, O., Shao, N., Kim, H.-M., Testori, S., Faull, P., Cutillas,
462 P., Snijders, A.P., Colaiácovo, M.P.*, et al.* (2018). Spatiotemporal regulation of Aurora B
463 recruitment ensures release of cohesion during C. elegans oocyte meiosis. Nature
464 Communications *9*, 834.
465 Foley, E.A., Maldonado, M., and Kapoor, T.M. (2011). Formation of stable attachments
466 between kinetochores and microtubules depends on the B56-PP2A phosphatase. Nature Cell
467 Biology *13*, 1265-1271.

468 Gelens, L., Qian, J., Bollen, M., and Saurin, A.T. (2018). The Importance of Kinase-
469 Phosphatase Integration: Lessons from Mitosis. Trends Cell Biol *28*, 6-21.
470 Hassold, T., and Hunt, P. (2001). To err (meiotically) is human: the genesis of human
471 aneuploidy. Nat Rev Genet *2*, 280-291.
472 Hattersley, N., Cheerambathur, D., Moyle, M., Stefanutti, M., Richardson, A., Lee, K.Y.,
473 Dumont, J., Oegema, K., and Desai, A. (2016). A Nucleoporin Docks Protein Phosphatase 1
474 to Direct Meiotic Chromosome Segregation and Nuclear Assembly. Dev Cell *38*, 463-477.
475 Hayward, D., Bancroft, J., Mangat, D., Alfonso-Pérez, T., Dugdale, S., McCarthy, J., Barr,
476 F.A., and Gruneberg, U. (2019). Checkpoint signaling and error correction require regulation
477 of the MPS1 T-loop by PP2A-B56. The Journal of Cell Biology, jcb.201905026.
478 Hertz, E.P.T., Kruse, T., Davey, N.E., Lopez-Mendez, B., Sigurethsson, J.O., Montoya, G.,
479 Olsen, J.V., and Nilsson, J. (2016). A Conserved Motif Provides Binding Specificity to the
480 PP2A-B56 Phosphatase. Molecular Cell *63*, 686-695.
481 Homer, H., Gui, L., and Carroll, J. (2009). A spindle assembly checkpoint protein functions in
482 prophase I arrest and prometaphase progression. Science *326*, 991-994.
483 Kaitna, S., Pasierbek, P., Jantsch, M., Loidl, J., and Glotzer, M. (2002). The aurora B kinase
484 AIR-2 regulates kinetochores during mitosis and is required for separation of homologous
485 Chromosomes during meiosis. Curr Biol *12*, 798-812.
486 Kettenbach, A.N., Schweppe, D.K., Faherty, B.K., Pechenick, D., Pletnev, A.A., and Gerber,
487 S.A. (2011). Quantitative phosphoproteomics identifies substrates and functional modules of
488 Aurora and Polo-like kinase activities in mitotic cells. Sci Signal *4*, rs5.
489 Kim, T., Lara-Gonzalez, P., Prevo, B., Meitinger, F., Cheerambathur, D.K., Oegema, K., and
490 Desai, A. (2017). Kinetochores accelerate or delay APC/C activation by directing Cdc20 to
491 opposing fates. Genes Dev *31*, 1089-1094.

492 Kim, T., Moyle, M.W., Lara-Gonzalez, P., De Groot, C., Oegema, K., and Desai, A. (2015).
493 Kinetochore-localized BUB-1/BUB-3 complex promotes anaphase onset in C. elegans. J Cell
494 Biol *209*, 507-517.
495 Kitagawa, D., Fluckiger, I., Polanowska, J., Keller, D., Reboul, J., and Gonczy, P. (2011).
496 PP2A phosphatase acts upon SAS-5 to ensure centriole formation in C. elegans embryos. Dev
497 Cell *20*, 550-562.
498 Kitajima, T.S., Sakuno, T., Ishiguro, K.-i., Iemura, S.-i., Natsume, T., Kawashima, S.A., and
499 Watanabe, Y. (2006). Shugoshin collaborates with protein phosphatase 2A to protect cohesin.
500 Nature *441*, 46-52.
501 Kruse, T., Gnosa, S.P., Nasa, I., Garvanska, D.H., Hein, J.B., Nguyen, H., Samsoe-Petersen,
502 J., Lopez-Mendez, B., Hertz, E.P.T., Schwarz, J.*, et al.* (2020). Mechanisms of site-specific
503 dephosphorylation and kinase opposition imposed by PP2A regulatory subunits. EMBO J,
504 e103695.
505 Kruse, T., Zhang, G., Larsen, M.S., Lischetti, T., Streicher, W., Kragh Nielsen, T., Bjorn,
506 S.P., and Nilsson, J. (2013). Direct binding between BubR1 and B56-PP2A phosphatase
507 complexes regulate mitotic progression. Journal of Cell Science *126*, 1086-1092.
508 Laband, K., Lacroix, B., Edwards, F., Canman, J.C., and Dumont, J. (2018). Methods in Cell
509 Biology, Vol 145.
510 Laband, K., Le Borgne, R., Edwards, F., Stefanutti, M., Canman, J.C., Verbavatz, J.M., and
511 Dumont, J. (2017). Chromosome segregation occurs by microtubule pushing in oocytes. Nat
512 Commun *8*, 1499.
513 Lange, K.I., Heinrichs, J., Cheung, K., and Srayko, M. (2013). Suppressor mutations identify
514 amino acids in PAA-1/PR65 that facilitate regulatory RSA-1/B″ subunit targeting of PP2A
515 to centrosomes in C. elegans. Biology open *2*, 88-94.

516 Magescas, J., Zonka, J.C., and Feldman, J.L. (2019). A two-step mechanism for the
517 inactivation of microtubule organizing center function at the centrosome. eLife *8*, e47867.
518 Marston, A.L., and Amon, A. (2004). Meiosis: cell-cycle controls shuffle and deal. Nat Rev
519 Mol Cell Biol *5*, 983-997.
520 Monen, J., Maddox, P.S., Hyndman, F., Oegema, K., and Desai, A. (2005). Differential role
521 of CENP-A in the segregation of holocentric C. elegans chromosomes during meiosis and
522 mitosis. Nature Cell Biology *7*, 1248.
523 Moura, M., and Conde, C. (2019). Phosphatases in Mitosis: Roles and Regulation.
524 Biomolecules *9*.
525 Moyle, M.W., Kim, T., Hattersley, N., Espeut, J., Cheerambathur, D.K., Oegema, K., and
526 Desai, A. (2014). A Bub1-Mad1 interaction targets the Mad1-Mad2 complex to unattached
527 kinetochores to initiate the spindle checkpoint. J Cell Biol *204*, 647-657.
528 Novak, B., Kapuy, O., Domingo-Sananes, M.R., and Tyson, J.J. (2010). Regulated protein
529 kinases and phosphatases in cell cycle decisions. Curr Opin Cell Biol *22*, 801-808.
530 Ohkura, H. (2015). Meiosis: an overview of key differences from mitosis. Cold Spring Harb
531 Perspect Biol *7*.
532 Padmanabhan, S., Mukhopadhyay, A., Narasimhan, S.D., Tesz, G., Czech, M.P., and
533 Tissenbaum, H.A. (2009). A PP2A regulatory subunit regulates C. elegans insulin/IGF-1
534 signaling by modulating AKT-1 phosphorylation. Cell *136*, 939-951.
535 Pal, S., Lant, B., Yu, B., Tian, R., Tong, J., Krieger, J.R., Moran, M.F., Gingras, A.C., and
536 Derry, W.B. (2017). CCM-3 Promotes C. elegans Germline Development by Regulating
537 Vesicle Trafficking Cytokinesis and Polarity. Curr Biol *27*, 868-876.
538 Pelisch, F., Bel Borja, L., Jaffray, E.G., and Hay, R.T. (2019). Sumoylation regulates protein
539 dynamics during meiotic chromosome segregation in *C. elegans* oocytes. Journal of Cell
540 Science *132*, jcs232330.

541 Pelisch, F., Tammsalu, T., Wang, B., Jaffray, E.G., Gartner, A., and Hay, R.T. (2017). A
542 SUMO-Dependent Protein Network Regulates Chromosome Congression during Oocyte
543 Meiosis. Mol Cell *65*, 66-77.
544 Qian, J., Garcia-Gimeno, M.A., Beullens, M., Manzione, M.G., Van der Hoeven, G., Igual,
545 J.C., Heredia, M., Sanz, P., Gelens, L., and Bollen, M. (2017). An Attachment-Independent
546 Biochemical Timer of the Spindle Assembly Checkpoint. Mol Cell *68*, 715-730 e715.
547 Riedel, C.G., Katis, V.L., Katou, Y., Mori, S., Itoh, T., Helmhart, W., Gálová, M., Petronczki,
548 M., Gregan, J., Cetin, B.*, et al.* (2006). Protein phosphatase 2A protects centromeric sister
549 chromatid cohesion during meiosis I. Nature *441*, 53-61.
550 Rogers, E., Bishop, J.D., Waddle, J.A., Schumacher, J.M., and Lin, R. (2002). The aurora
551 kinase AIR-2 functions in the release of chromosome cohesion in Caenorhabditis elegans
552 meiosis. J Cell Biol *157*, 219-229.
553 Schindelin, J., Arganda-Carreras, I., Frise, E., Kaynig, V., Longair, M., Pietzsch, T.,
554 Preibisch, S., Rueden, C., Saalfeld, S., Schmid, B.*, et al.* (2012). Fiji: an open-source platform
555 for biological-image analysis. Nat Methods *9*, 676-682.
556 Schlaitz, A.-L., Srayko, M., Dammermann, A., Quintin, S., Wielsch, N., MacLeod, I., de
557 Robillard, Q., Zinke, A., Yates, J.R., Müller-Reichert, T.*, et al.* (2007). The C. elegans RSA
558 Complex Localizes Protein Phosphatase 2A to Centrosomes and Regulates Mitotic Spindle
559 Assembly. Cell *128*, 115-127.
560 Schlientz, A.J., and Bowerman, B. (2020). C. elegans CLASP/CLS-2 negatively regulates
561 membrane ingression throughout the oocyte cortex and is required for polar body extrusion.
562 PLoS Genet *16*, e1008751.
563 Schumacher, J.M., Golden, A., and Donovan, P.J. (1998). AIR-2: An Aurora/Ipl1-related
564 protein kinase associated with chromosomes and midbody microtubules is required for polar

565 body extrusion and cytokinesis in Caenorhabditis elegans embryos. J Cell Biol *143*, 1635-
566 1646.
567 Seshacharyulu, P., Pandey, P., Datta, K., and Batra, S.K. (2013). Phosphatase: PP2A
568 structural importance, regulation and its aberrant expression in cancer. Cancer Letters *335*, 9-
569 18.
570 Shi, Y. (2009). Serine/threonine phosphatases: mechanism through structure. Cell *139*, 468-
571 484.
572 Sieburth, D.S., Sundaram, M., Howard, R.M., and Han, M. (1999). A PP2A regulatory
573 subunit positively regulates Ras-mediated signaling during Caenorhabditis elegans vulval
574 induction. Genes Dev *13*, 2562-2569.
575 Sievers, F., Wilm, A., Dineen, D., Gibson, T.J., Karplus, K., Li, W., Lopez, R., McWilliam,
576 H., Remmert, M., Soding, J.*, et al.* (2011). Fast, scalable generation of high-quality protein
577 multiple sequence alignments using Clustal Omega. Mol Syst Biol *7*, 539.
578 Song, M.H., Liu, Y., Anderson, D.E., Jahng, W.J., and O'Connell, K.F. (2011). Protein
579 phosphatase 2A-SUR-6/B55 regulates centriole duplication in C. elegans by controlling the
580 levels of centriole assembly factors. Dev Cell *20*, 563-571.
581 Sonneville, R., and Gonczy, P. (2004). Zyg-11 and cul-2 regulate progression through meiosis
582 II and polarity establishment in C. elegans. Development *131*, 3527-3543.
583 Suijkerbuijk, S.J., Vleugel, M., Teixeira, A., and Kops, G.J. (2012). Integration of kinase and
584 phosphatase activities by BUBR1 ensures formation of stable kinetochore-microtubule
585 attachments. Dev Cell *23*, 745-755.
586 Tang, Z., Shu, H., Qi, W., Mahmood, N.A., Mumby, M.C., and Yu, H. (2006). PP2A Is
587 Required for Centromeric Localization of Sgo1 and Proper Chromosome Segregation.
588 Developmental Cell *10*, 575-585.

589 Timmons, L., Court, D.L., and Fire, A. (2001). Ingestion of bacterially expressed dsRNAs can
590 produce specific and potent genetic interference in Caenorhabditis elegans. Gene *263*, 103-
591 112.
592 Timmons, L., and Fire, A. (1998). Specific interference by ingested dsRNA. Nature *395*, 854.
593 Touati, S.A., Buffin, E., Cladiere, D., Hached, K., Rachez, C., van Deursen, J.M., and
594 Wassmann, K. (2015). Mouse oocytes depend on BubR1 for proper chromosome segregation
595 but not for prophase I arrest. Nat Commun *6*, 6946.
596 Tzur, Y.B., Egydio de Carvalho, C., Nadarajan, S., Van Bostelen, I., Gu, Y., Chu, D.S.,
597 Cheeseman, I.M., and Colaiacovo, M.P. (2012). LAB-1 targets PP1 and restricts Aurora B
598 kinase upon entrance into meiosis to promote sister chromatid cohesion. PLoS Biol *10*,
599 e1001378.
600 UniProt, C. (2019). UniProt: a worldwide hub of protein knowledge. Nucleic Acids Res *47*,
601 D506-D515.
602 Vallardi, G., Allan, L.A., Crozier, L., and Saurin, A.T. (2019). Division of labour between
603 PP2A-B56 isoforms at the centromere and kinetochore. eLife *8*, e42619.
604 Van Roey, K., and Davey, N.E. (2015). Motif co-regulation and co-operativity are common
605 mechanisms in transcriptional, post-transcriptional and post-translational regulation. Cell
606 Communication and Signaling *13*, 45.
607 Wang, R., Kaul, Z., Ambardekar, C., Yamamoto, T.G., Kavdia, K., Kodali, K., High, A.A.,
608 and Kitagawa, R. (2013). HECT-E3 ligase ETC-1 regulates securin and cyclin B1
609 cytoplasmic abundance to promote timely anaphase during meiosis in C. elegans.
610 Development *140*, 2149-2159.
611 Wang, S., Wu, D., Quintin, S., Green, R.A., Cheerambathur, D.K., Ochoa, S.D., Desai, A.,
612 and Oegema, K. (2015). NOCA-1 functions with gamma-tubulin and in parallel to Patronin to
613 assemble non-centrosomal microtubule arrays in C. elegans. Elife *4*, e08649.

614 Wang, X., Bajaj, R., Bollen, M., Peti, W., and Page, R. (2016). Expanding the PP2A
615 Interactome by Defining a B56-Specific SLiM. Structure *24*, 2174-2181.
616 Waterhouse, A.M., Procter, J.B., Martin, D.M., Clamp, M., and Barton, G.J. (2009). Jalview
617 Version 2--a multiple sequence alignment editor and analysis workbench. Bioinformatics *25*,
618 1189-1191.
619 Xu, P., Raetz, E.A., Kitagawa, M., Virshup, D.M., and Lee, S.H. (2013). BUBR1 recruits
620 PP2A via the B56 family of targeting subunits to promote chromosome congression. Biology
621 Open *2*, 479.
622 Xu, P., Virshup, D.M., and Lee, S.H. (2014). B56-PP2A regulates motor dynamics for mitotic
623 chromosome alignment. Journal of Cell Science *127*, 4567.
624 Xu, Y., Chen, Y., Zhang, P., Jeffrey, P.D., and Shi, Y. (2008). Structure of a Protein
625 Phosphatase 2A Holoenzyme: Insights into B55-Mediated Tau Dephosphorylation. Molecular
626 Cell *31*, 873-885.
627 Xu, Y., Xing, Y., Chen, Y., Chao, Y., Lin, Z., Fan, E., Yu, J.W., Strack, S., Jeffrey, P.D., and
628 Shi, Y. (2006). Structure of the Protein Phosphatase 2A Holoenzyme. Cell *127*, 1239-1251.
629 Xu, Z., Cetin, B., Anger, M., Cho, U.S., Helmhart, W., Nasmyth, K., and Xu, W. (2009).
630 Structure and Function of the PP2A-Shugoshin Interaction. Molecular Cell *35*, 426-441.
631 Yoshida, S., Kaido, M., and Kitajima, T.S. (2015). Inherent Instability of Correct
632 Kinetochore-Microtubule Attachments during Meiosis I in Oocytes. Dev Cell *33*, 589-602.
633

634 **METHODS**

635 ***C. elegans* strains**

636 Strains used in this study were maintained at 20 degrees unless indicated otherwise. For a
637 complete list of strains, please refer to Supplementary Table 2. Requests for strains not
638 deposited in the CGC should be done through the FP lab's website
639 (https://pelischlab.co.uk/reagents/).

640 **RNAi**

641 For RNAi experiments, we cloned the different sequences in the L4440 RNAi feeding vector
642 (Timmons and Fire, 1998).
643 All sequences were inserted into L4440 using the NEBuilder HiFi DNA Assembly Master
644 Mix (New England Biolabs) and transformed into DH5a bacteria. The purified plasmids were
645 then transformed into HT115(DE3) bacteria (Timmons et al., 2001). RNAi clones were
646 picked and grown overnight at 37°C in LB with 100 µg/ml ampicillin. Saturated cultures were
647 diluted 1:100 and allowed to grow until reaching an OD_{600} of 0.6–0.8. IPTG (isopropyl-β-d-
648 thiogalactopyranoside) was added to a final concentration of 1 mM and cultures were
649 incubated overnight at 20°C. Bacteria were then seeded onto NGM plates made with agarose
650 and allowed to dry. L4 worms were then plated on RNAi plates and grown to adulthood at
651 20°C for 24 hs in the case of *let-92(RNAi)*, *bub-1(RNAi)*, and *paa-1(RNAi)*, and 48 hs in all
652 other cases.

653 **CRISPR strains**

654 GFP::SUR-6

655 For the generation of in situ-tagged GFP::SUR-6, we used the Self-Excising Cassette method
656 (Dickinson et al., 2015). In brief, N2 adults were injected with a plasmid mix containing
657 Cas9, a sgRNA targeting the N-terminus of sur-6 and a repairing template to insert the GFP
658 sequence, along with a LoxP-flanked cassette that encoded for a hygromycin resistance gene,

659 a sqt-1 mutant to confer a dominant roller phenotype, and heat-shocked-induced Cre
660 recombinase. After selection in hygromycin, positive integrants (evidenced by their roller
661 phenotype) were heat-shocked to express Cre and remove the cassette.
662
663 The strains AID::GFP::GSP-2, GFP::PAA-1, BUB-1^{K718R,D847N}, and BUB-1^{L282A,V285A} were
664 generated by Sunybiotech.
665 AID::GFP::GSP-2
666 (AID in purple, GFP in green, synonimous mutations in cyan)
667 ATGCCTAAAGATCCAGCCAAACCTCCGGCCAAGGCACAAGTTGTGGGATGGCCA
668 CCGGTGAGATCATACCGGAAGAACGTGATGGTTTCCTGCCAAAAATCAAGCGGT
669 GGCCCGGAGGCGGCGGCGTTCGTGAAGAGTAAAGGAGAAGAACTTTTCACTGGA
670 GTTGTCCCAATTCTTGTTGAATTAGATGGTGATGTTAATGGGCACAAATTTTCTGT
671 CAGTGGAGAGGGTGAAGGTGATGCAACATACGGAAAACTTACCCTTAAATTTATT
672 TGCACTACTGGAAAACTACCTGTTCCATGGgtaagtttaaacatatatatactaactaaccctgattatttaaat
673 tttcagCCAACACTTGTCACTACTTTCTgTTATGGTGTTCAATGCTTcTCgAGATACCCA
674 GATCATATGAAACgGCATGACTTTTTCAAGAGTGCCATGCCCGAAGGTTATGTAC
675 AGGAAAGAACTATATTTTTCAAAGATGACGGGAACTACAAGACACgtaagtttaaacagtt
676 cggtactaactaaccatacatatttaaattttcagGTGCTGAAGTCAAGTTTGAAGGTGATACCCTTGTT
677 AATAGAATCGAGTTAAAAGGTATTGATTTTAAAGAAGATGGAAACATTCTTGGAC
678 ACAAATTGGAATACAACTATAACTCACACAATGTATACATCATGGCAGACAAAC
679 AAAAGAATGGAATCAAAGTTgtaagtttaaacatgattttactaactaactaatctgatttaaattttcagAACTTC
680 AAAATTAGACACAACATTGAAGATGGAAGCGTTCAACTAGCAGACCATTATCAA
681 CAAAATACTCCAATTGGCGATGGCCCTGTCCTTTTACCAGACAACCATTACCTGT
682 CCACACAATCTGCCCTTTCGAAAGATCCCAACGAAAAGAGAGACCACATGGTCCT

683 TCTTGAGTTTGTAACAGCTGCTGGGATTACACATGGCATGGATGAACTATACAAA

684 GACGTAGAAAAGCTTAATCTCGACAATATCATCTCCAGATTATTGGAAG.

685

686 GFP::PAA-1

687 (GFP in green, synonimous mutations in cyan)

688 ATGAGTAAAGGAGAAGAACTTTTCACTGGAGTTGTCCCAATTCTTGTTGAATTAG

689 ATGGTGATGTTAATGGGCACAAATTTTCTGTCAGTGGAGAGGGTGAAGGTGATGC

690 AACATACGGAAAACTTACCCTTAAATTTATTTGCACTACTGGAAAACTACCTGTT

691 CCATGGgtaagtttaaacatatatatactaactaaccctgattatttaaattttcagCCAACACTTGTCACTACTTTC

692 TgTTATGGTGTTCAATGCTTcTCgAGATACCCAGATCATATGAAACgGCATGACTTT

693 TTCAAGAGTGCCATGCCCGAAGGTTATGTACAGGAAAGAACTATATTTTTCAAAG

694 ATGACGGGAACTACAAGACACgtaagtttaaacagttcggtactaactaaccatacatatttaaattttcagGTGC

695 TGAAGTCAAGTTTGAAGGTGATACCCTTGTTAATAGAATCGAGTTAAAAGGTATT

696 GATTTTAAAGAAGATGGAAACATTCTTGGACACAAATTGGAATACAACTATAACT

697 CACACAATGTATACATCATGGCAGACAAACAAAAGAATGGAATCAAAGTTgtaagttt

698 aaacatgattttactaactaactaatctgatttaaattttcagAACTTCAAAATTAGACACAACATTGAAGATG

699 GAAGCGTTCAACTAGCAGACCATTATCAACAAAATACTCCAATTGGCGATGGCCC

700 TGTCCTTTTACCAGACAACCATTACCTGTCCACACAATCTGCCCTTTCGAAAGATC

701 CCAACGAAAAGAGAGACCACATGGTCCTTCTTGAGTTTGTAACAGCTGCTGGGAT

702 TACACATGGCATGGATGAACTATACAAAGGAGGTGGATCCGGTGGTGGATCCTC

703 GGTTGTCGAAGAAGCTACTGACGACGCG.

704

705 *bub-1*^{K718R,D847N}

706 The wild type sequence:

707 GTAACCGATGATCAAAGGACAGTAGCTGTGAAGTACGAGGTGCCATCATGTTCGT

708 GGGAAGTGTACATTTGCGACCAAATGCGGAATCGCCTGAAAGATCGAGGTTTGG

709 AGCTGATGGCCAAATGTTGCATTATGGAAGTGATGGATGCTTATGTTTATTCAAC

710 TGCTTCGCTTCTTGTTAATCAGTACCACGAATATGGAACGCTGCTTGAATATGCG

711 AATAACATGAAGGATCCGAATTGGCACATAACCTGCTTCTTGATTACCCAAATGG

712 CCCGAGTTGTGAAGGAAGTCCATGCCTCTAAAATTATTCATGGAGATATCAAACC

713 GGATAATTTTATGATCACCAGAAAgtatgggaaaacatttgttaattttagacgttatctttttcagGATCGA

714 TGATAAATGGGGCAAAGATGCTCTGATGAGTAACGACAGCTTTGTCATCAAGATT

715 ATCGACTGGGGACGTGCCATTGACATGATGCCACTGAAGAACCAGCGT

716 was mutated to:

717 GTAACCGATGATCAAAGGACAGTAGCTGTGCGCTACGAGGTGCCATCATGTTCGT

718 GGGAAGTGTACATTTGCGACCAAATGCGGAATCGCCTGAAAGATCGAGGTTTGG

719 AGCTGATGGCCAAATGTTGCATTATGGAAGTGATGGATGCTTATGTTTATTCAAC

720 TGCTTCGCTTCTTGTTAATCAGTACCACGAATATGGAACGCTGCTTGAATATGCG

721 AATAACATGAAGGATCCGAATTGGCACATAACCTGCTTCTTGATTACCCAAATGG

722 CCCGAGTTGTGAAGGAAGTCCATGCCTCTAAAATTATTCATGGAGATATCAAACC

723 GGATAATTTTATGATCACCAGAAAgtatgggaaaacatttgttaattttagacgttatctttttcagGATCGA

724 TGATAAATGGGGCAAAGATGCTCTGATGAGTAACGACAGCTTTGTCATCAAGATT

725 ATCAATTGGGGACGTGCGATTGACATGATGCCACTGAAGAACCAGCGT

726 The introduced changes are shown in red and synonymous mutations are shown in cyan.

727

728 *bub-1*^{L282A,V285A}

729 The wild type sequence:

730 AACGCCAATCTAAATCCTAGAAGACGTCATCTTTCACCAGTCAGTGAGAAAACGG

731 TTGATGATGAGGAGGAAAAG

732 was mutated to:

733 AACGCCAATCTAAATCCTAGAAGACGTCATGCATCACCAGCTAGCGAGAAAACG

734 GTTGATGATGAGGAGGAAAAG

735 The introduced changes are shown in red and synonymous mutations are shown in cyan.

736 See Supplementary Table 3 for the primer sequences used for genotyping.

737

738 **Live imaging of oocytes**

739 A detailed protocol for live imaging of *C. elegans* oocytes was used with minor modifications

740 (Laband et al., 2018). Fertilized oocytes were dissected and mounted in 5 µl of L-15

741 blastomere culture medium (0.5 mg/mL Inulin; 25 mM HEPES, pH 7.5 in 60% Leibowitz L-

742 15 medium and 20% heat-Inactivated FBS) on 24×40 mm #1.5 coverslips. Once dissection

743 was performed and early oocytes identified using a stereomicroscope, a circle of Vaseline was

744 laid around the sample, and a custom-made 24×40 mm plastic holder (with a centred window)

745 was placed on top. The sample was imaged immediately. Live imaging was done using a

746 60X/NA 1.4 oil objective on a spinning disk confocal microscope (MAG Biosystems)

747 mounted on a microscope (IX81; Olympus), an EMCCD Cascade II camera (Photometrics),

748 spinning-disk head (CSU-X1; Yokogawa Electric Corporation). Acquisition parameters were

749 controlled by MetaMorph 7 software (Molecular Devices). Images were acquired every 20

750 seconds (with the exception of Figures 1B, 3C, and S1A, where a 30-second interval was

751 used). For all live imaging experiments, partial max-intensity projections are presented in the

752 figures and full max-intensity projections are presented in the supplementary movies. All files

753 were stored, classified, and managed using OMERO (Allan et al., 2012). Figures were

754 prepared using OMERO.figure and assembled using Adobe Illustrator. Representative movies

755 shown in Supplementary material were assembled using custom-made macros in Fiji/ImageJ

756 (Schindelin et al., 2012).

757 **Generation of phospho-Ser 283 BUB-1 antibody.**

758 The antibody was generated by Moravian Biotec by immunising rabbits with the following
759 peptide: RRRHL(pS)PVSEKTC. Serum was adsorbed with a non-phosphorylated peptide
760 (RRRHLSPVSEKTC) followed by affinity purification with the antigenic, phosphorylated
761 peptide. Different fractions were tested in immunofluorescence by incubating different
762 dilutions (1:1,000 & 1:10,000) with 1 µM and 10 µM of either non-phosphorylated or
763 phosphorylated peptide. Only the phosphorylated peptide compited out the signal.
764 Additionally, we used the BUB-1^{S283A} strain and no antibody signal was detected.

765 **Immunofluorescence**

766 Worms were placed on 4 µl of M9 worm buffer in a poly-D-lysine (Sigma, P1024)-coated
767 slide and a 24×24-cm coverslip was gently laid on top. Once the worms extruded the
768 embryos, slides were placed on a metal block on dry ice for >10 min. The coverslip was then
769 flicked off with a scalpel blade, and the samples were fixed in methanol at 20°C for 30 min.
770 After blocking in PBS buffer plus 3% BSA and 0.1% Triton X-100 (AbDil), samples were
771 incubated overnight at 4°C with anti-BUB-1 (Desai et al., 2003) and anti-tubulin (1/400,
772 clone DM1α, Sigma Aldrich) in AbDil. After three washes with PBS plus 0.1% Tween,
773 secondary antibodies were added at 1/1000 (goat anti-mouse and goat anti-rabbit conjugated
774 to Alexa Fluor™ 488, Alexa Fluor™ 594, Thermo Scientific). After two hours at room
775 temperature and three washes with PBS plus 0.1% Tween, embryos were mounted in
776 ProLong Diamond antifade mountant with DAPI (Thermo Scientific).
777 For the comparisson of total versus phospho-Ser 283 BUB-1, a total BUB-1 antibody was
778 labelled with Alexa-488 while phospho-Ser 283 BUB-1 was labelled with Alexa 647, using
779 the APEX™ Alexa Fluor™ Antibody Labelling kits (Thermo). We used the strain HY604,
780 which is a temperature-sensitive allele of the the APC component MAT-1, that arrests in
781 meiosis I prior to spindle rotation when moved to the restrictive temperature.

782 **GFP immunoprecipitation**

783 For GFP immunoprecipitations, we followed a published protocol (Sonneville et al., 2017)
784 with minor modifications (Pelisch et al., 2019). Approximately 1000 worms expressing GFP-
785 tagged endogenous BUB-1 were grown for two generations at 20°C in large 15-cm NGM
786 plates with concentrated HT115 bacteria. Worms were bleached and embryos were laid in
787 new 15-cm NGM plates with concentrated HT115 bacteria. Once >80% of the worm
788 population was at the L3/L4 stage, worms were washed and placed on 15-cm agarose plates
789 containing concentrated HT115 bacteria. After 24 hs, worms were bleached and the embryos
790 were resuspended in a lysis buffer containing 100 mM HEPES-KOH pH 7.9, 50 mM
791 potassium acetate, 10 mM magnesium acetate, 2 mM EDTA, 1X Protease inhibitor ULTRA
792 (Roche), 2X PhosSTOP (Roche), and 1 mM DTT. The solution was added drop-wise to liquid
793 nitrogen to generate beads that were later grinded using a SPEX SamplePrep 6780
794 Freezer/Mill. After thawing, we added one-quarter volume of buffer containing lysis buffer
795 supplemented with 50% glycerol, 300 mM potassium acetate, 0.5% NP40, plus DTT, protease
796 and phosphatase inhibitors as above. DNA was digested with 1,600U of Pierce Universal
797 Nuclease for 30 min on ice. Extracts were centrifuged at 25,000 g for 30 min and then at
798 100,000 g for 1 h. The extract was then incubated for 60 min with 30 µl of a GFP nanobody
799 covalently coupled to magnetic beads. The beads were washed ten times with 1 ml of wash
800 buffer (100 mM HEPES-KOH pH 7.9, 300 mM potassium acetate, 10 mM magnesium
801 acetate, 2 mM EDTA, 0.1% NP40, plus protease and phosphatase inhibitors) at 4°C (cold
802 room). Bound proteins were eluted twice using two rounds of 50 µl LDS sample buffer
803 (Thermo Scientific) at 70°C for 15 min and stored at −80°C.

804

805 **Sample preparation for mass spectrometry**

806 IP samples were run onm 4-12% Bis-Tris SDS gels with MOPS running buffer and the gel
807 was stained using Quick Coomassie Stain (Generon). Bands of interest were cut and washed
808 with water:acetonitrile (50:50), followed by a wash with 100 mM ammonium bicarbonate.
809 The gel pieces were then washed with 100 mM ammonium bicarbonate:acetonitrile (50:50),
810 followed by a final wash with acetonitrile. Gel pieces were dried using a SpeedVac.
811 Samples were reduced with 10mM DTT in 20 mM ammonium bicarbonate and alkilated
812 With 50 mM IAA in 20 mM ammonium bicarbonate. Samples were then washed sequentially
813 with 100 mM ammonium bicarbonate, 100 mM ammonium bicarbonate:Acetonitrile (50:50),
814 and acetonitrile. Gel pieces were dried using a SpeedVac.
815 Trypsin solution (12.5 µg/ml stock in 20 mM ammonium bicarbonate) was added to cover the
816 gel pieces and and incubated for 30 mins on a shaking platform and incubated sample
817 overnight at 30ºC on a shaker. Peptides were extracted by standard procedures and
818 reconstituted in 10 µl of 5% formic acid/10% acetonitrile. After vortexing for 1 min, water
819 was added to 50 µl.
820
821 **Mass Spectrometry analysis**
822 Samples were run on an Ultimate 3000 RSLCnano system (ThermoFisher Scientific) coupled
823 to a Q-Exactive Plus Mass Spectrometer (Thermo Fisher Scientific). Peptides initially trapped
824 on an Acclaim PepMap 100 (Thermo Fisher Scientific) and then separated on an Easy-Spray
825 PepMap RSLC C18 column (Thermo Fisher Scientific). Sample was transferred to mass
826 spectrometer via an Easy-Spray source with temperature set at 50˚C and a source voltage of
827 2.1 kV. The mass spectrometer was operated on in data dependent acquisition mode (top 15
828 method). MS resolution was 70,000 with a mass range of 350 to 1600. MS/MS resolution was
829 17,500.

830 .RAW data files were extracted and converted to mascot generic files (.mgf) using MSC
831 Convert. Extracted data then searched against *Caenorhabditis elegans* proteome and BUB-1
832 specifically, using the Mascot Search Engine (Mascot Daemon Version 2.3.2). Type of search
833 used was MS/MS Ion Search, using Trypsin/P. Carbamidomethyl (C) was set as a fixed
834 modification and variable modifications were as follows: acetyl (N-term), dioxidation (M),
835 Gln to pyro-Glu (N-term Q), Oxidation (M), Deamidation (NQ), and Phosphorylation (STY).
836 Peptide Mass Tolerance was ± 10 ppm (# 13C = 2) with a Fragment Mass Tolerance of ± 0.6
837 Da. Maximum number of missed cleavages was 2.
838
839 **Sequence Alignment**
840 All sequence alignments were performed using Clustal Omega (Sievers et al., 2011), version
841 1.2.4. Full-length mammalian B56α (UniProtKB Q15172), β (UniProtKB Q15173), γ
842 (UniProtKB Q13362), δ (UniProtKB Q14738) and ε (UniProtKB Q16537) alongside their
843 alternative splicing isoforms were retrieved from UniProt (Bateman et.al., 2017) and aligned
844 with full-length *C. elegans* PPTR-1 (UniProtKB O18178) and PPTR-2 (UniProtKB A9UJN4-
845 1). A guide tree was calculated from the distance matrix generated from sequence pairwise
846 scores.
847
848 The C-terminal regions of mammalian isoforms B56γ (S378-A393), δ (S454-A469), β (S409-
849 V424), α (S403-V418), ε (S395-V410) and *C. elegans* PPTR-1 (S420-V435) and PPTR-2
850 (S449-A464) were used for the alignment. The canonical sequences of each B56 isoform were
851 retrieved from UniProt (UniProt, 2019).
852
853 The short linear motifs (SLiMs) of *C. elegans* BUB-1 (R279-D292;UniProtKB Q21776),
854 human BubR1 (I666-A679;UniProtKB O60566-1) and RepoMan (K587-P600; UniProtKB

855 Q69YH5-1) were aligned with Clustal Omega (Sievers et al., 2011) and visualised with
856 Jalview (Waterhouse et al., 2009).
857
858 **Kinase assays**
859 Forty µl reactions were set up containing 40 mM Tris-HCl pH 7.5, 100 µM ATP, 10 mM
860 $MgCl_2$, and 2 µg of either BUB-1 (259-332) or H1. At t=0, 15 ng/µl Cdk1/Cyclin B was
861 added, before incubation at 30ºC for 30 min. Aliquots were taken immediately after
862 Cdk1/CyclinB addition at t=0 and then again after the 30 min incubation. All samples were
863 then incubated at 70ºC for 15 mins in a final concentration of 1X LDS buffer. SDS-PAGE
864 was then conducted on a NuPage 4-12% Bis-Tris gel (Thermo) with MES buffer before being
865 stained with ProQ Diamond (Thermo) and imaged using Bio-Rad ChemiDoc. Once
866 fluorescence was recorded, Coomassie staining was performed. For the western blot, SDS-
867 PAGE was conducted as above with 67 ng of substrate protein per well before the western
868 was conducted using a nitrocellulose membrane (GE healthcare) and 1X NuPage transfer
869 buffer (Thermo). The membrane was blocked using Intercept PBS blocking buffer (LI-COR),
870 the primary antibodies used were anti-GST at 1:1,000 (made in sheep), and anti- phospho-Ser
871 283 1:20,000 (made in rabbit). Secondary antibodies were anti-sheep IRDye 680RD anti-
872 rabbit 800CW (LI-COR),both at 1:50,000. The membrane was then imaged using LI-COR
873 Odyssey CLx.
874
875 **Expression and purification of PPTR-2**
876 PPTR-2 was expressed from pHISTEV30a vector as a 6xHis- and Strep-tagged protein
877 (plasmid fgp_445) in E. coli strain BL21 (DE3) and the bacterial culture was incubated
878 overnight at 37ºC with shaking at 220 rpm. Bacteria were grown in TB medium at 37°C with
879 shaking at 220 rpm until OD600 reached ~0.6 -0.8 and induced with 150 µM IPTG. Induction

880 was performed at 18°C with shaking at 220 rpm for ~16 hours. Cells were pelleted and lysed
881 by sonication in 50 mM NaP, 300 mM NaCl, 10 mM imidazole, 10% Glycerol, 0.5 mM
882 TCEP, and protease inhibitors. After binding to a Ni-NTA column, protein was washed with
883 20 mM imidazole and then eluted with 350 mM imidazole. The tag was cleaved with 6xHis-
884 tagged TEV protease overnight at 4°C and the tag and protease were removed from the
885 sample by binding to Ni-NTA. PPTR-2 was concentrated and further purified using a HiLoad
886 16/600 Superdex 200 pg size exclusion column.
887
888 **Fluorescence Polarisation**
889 The following peptides were synthesised by peptides&elephants GmbH: BUB-1 FITC-Ahx-
890 NPRRRHLSPVSEKTVDDEEE, pBUB-1 FITC-Ahx-NPRRRHLphSPVSEKTVDDEEE, and
891 LAVA FITC-Ahx-NPRRRHASPASEKTVDDEEE. Reactions (35 µl) were set up in FP
892 buffer (50 mM NaP pH 7.5, 150 mM NaCl, 0.5 mM TCEP) containing peptide concentrations
893 of 1 µM. These were then used to create a 1:2 serial dilution series using FP buffer
894 containing the same peptide concentrations as above as well as ~208 µM PPTR-2. The
895 reactions were left for 30 min before triplicates of each dilution were aliquoted into a black
896 384-well plate, centrifuged (2 min, 2000 rpm), and analysed using the PheraStar FS.
897
898 **Image analysis and Statistics**
899 For time-dependent analysis, metaphase I was taken as time = 0 seconds. This frame was
900 chosen as the previous frame where the first indication of chromosome separation was visible.
901 All image analysis was done in Fiji (Schindelin et al., 2012). For total intensity measurements
902 within the meiotic spindle, images were thresholded and binary images were generated using
903 the ReinyEntropy method and used to automatically generate the regions of interest (ROIs)
904 for each slice (z) and time point (t) or in the sum-projected image. Going through all the slices

905 was particularly necessary when measuring protein intensity associated with a specific
906 structure/location, since the angle of the spindle can lead to erroneous analysis. All ROIs were
907 recorded and, in order to get background measurements, the ROIs were automatically placed
908 on a different oocyte region, away from the spindle. Background-substracted intensity values
909 were then normalised to the maximum intensity value of the control movie using Graphpad
910 Prism 7.0 and are presented as mean ± s.e.m.
911
912 Central spindle to chromosome ratio for PPTR-2::GFP (Figure 4G) were obtained as follows.
913 Images were selected at early anaphase (t = 40 sec) and to obtain the chromosome ROIs, we
914 used the mCherry::histone channel to create a mask. These ROIs were transferred to the
915 PPTR-2::GFP channel and the intensity was measured as above. The region between the
916 chromosomes was selected intensities were measured to obtain the central spindle intensity.
917 Background corrected values were used to obtain the ratio central spindle/chromosome.
918 Results are shown as median with interquartile range and differences were analysed using an
919 unpaired two-tailed t-test with Welch's correction.
920
921 For the alignment/congression analysis, we selected movies in which the spindles were
922 contained in a single Z-plane at -80 sec. There, we established the spindle axes with a line
923 extending from pole to pole and the 'metaphase plate' with a perpendicular line in the middle
924 of the spindle (See Figure S5). A line was drawn on the long axes of the bivalents and the
925 angle between this line and the spindle axis was measured ('θ'). Additionally, for each
926 bivalent, the distance ('d') between the center of the bivalent and the metaphase plate was
927 measured.
928

929 Contingency tables were analysed using the Fisher's exact test (two-tailed) and the P values
930 are presented in the figures and/or in the text.
931
932 **Generation of Supplementary movies**
933 The 4D TIFF files were converted to movie (.avi) files using a custom-made macro that uses
934 the StackReg Fiji plugin for image registration. Movies were assembled using max intensity
935 projections hence the movies might not match a specific panel within the main figures, which
936 are single slices or partial projections in order to highlight specific characteristics.

Bel Borja et al. Figure 1

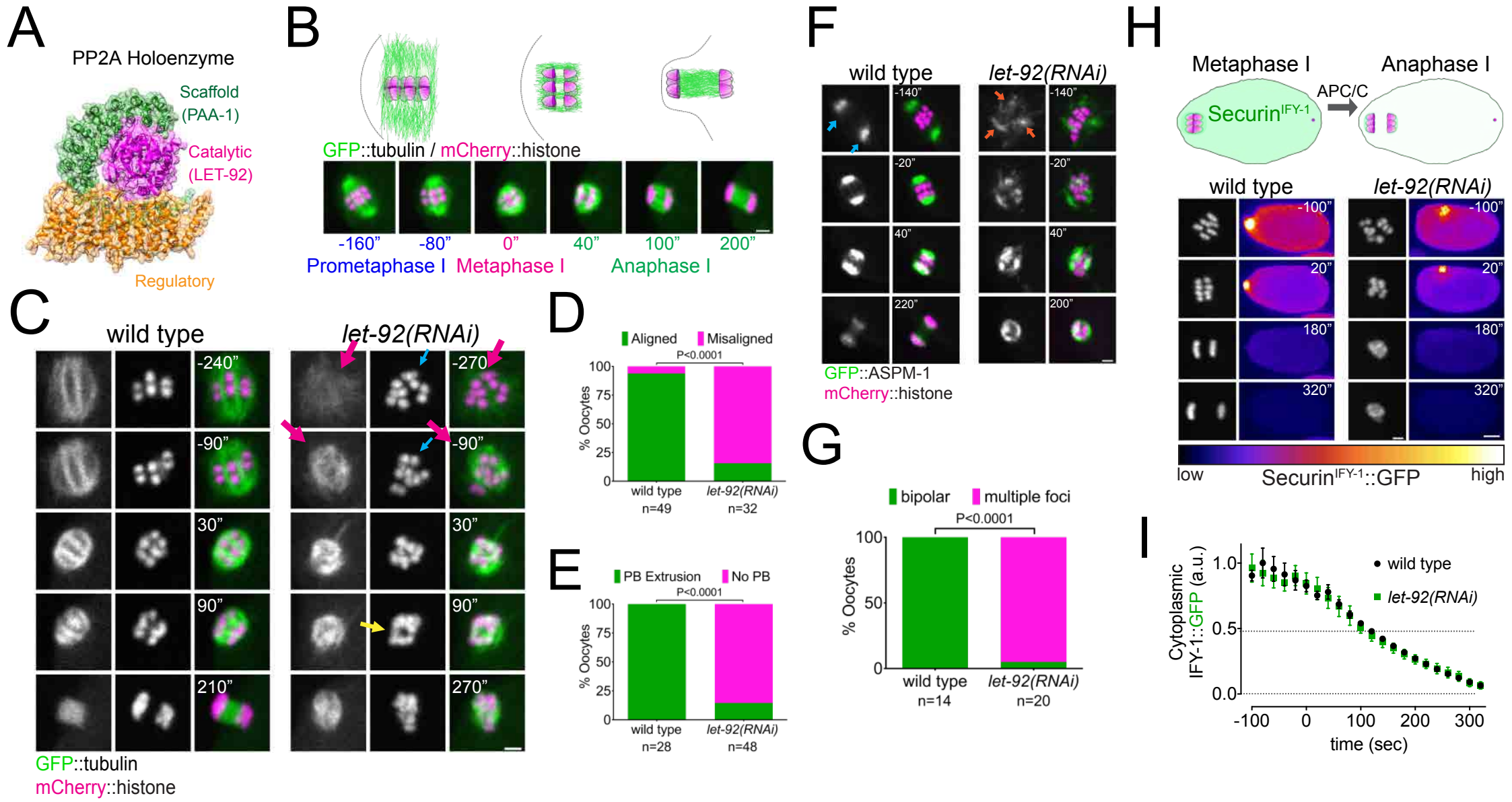

Figure 1. PP2A is essential for Meiosis I in *C. elegans* oocytes.

A. Schematic of the PP2A heterotrimer highlighting the single catalytic and scaffold subunits in *C. elegans* (LET-92 and PAA-1, respectively). The schematic was generated from the PDB structure 2npp (Xu et al., 2006).

B. Schematic of the timescales used throughout the paper. Metaphase I was defined as time zero and chosen as the frame prior to the one where chromosome separation was detected.

C. Microtubule and chromosome dynamics were followed in wild type and *let-92(RNAi)* oocytes expressing GFP::tubulin and mCherry::histone. Magenta arrows point to defective spindle structure; the cyan arrow points to misaligned chromosomes; the yellow arrow shows an apparent separation between chromosome masses. Inset numbers represent the time relative to metaphaseI in seconds. Scale bar, 2 µm. See Supp. Movie 1.

D. The number of oocytes with misaligned chromosomes in metaphase I was compared between wild type and *let-92(RNAi)* oocytes and the percentage is represented ($P<0.0001$, Fisher's exact test). The number of oocytes analysed (n) is shown.

E. The number of oocytes with an extruded polar body (PB) after meiosis I in wild type and *let-92(RNAi)* oocytes was analysed and the percentage is represented ($P<0.0001$, Fisher's exact test). The number of oocytes analysed (n) is shown.

F. ASPM-1 and chromosome dynamics were followed in wild type and *let-92 (RNAi)* oocytes expressing GFP::ASPM-1 and mCherry::histone. Inset numbers represent the time relative to metaphase I in seconds. Cyan arrows point to spindle poles whereas orange arrows highlight the unfocused ASPM-1 cumuli. Scale bar, 2 µm. See Supp. Movie 2.

G. The number of oocytes with defective spindle at prometaphase I in wild type and *let-92(RNAi)* oocytes was analysed and the percentage is represented ($P<0.0001$, Fisher's exact test). The number of oocytes analysed (n) is shown.

H. Securin^{IFY-1} degradation was used as a proxy for anaphase progression and followed in wild type and *let-92(RNAi)* oocytes. Greyscale images of the chromosomes are shown as well as whole oocyte images using the 'fire' LUT. The intensity scale is shown in the bottom. Inset numbers represent the time relative to metaphaseI in seconds. Scale bar, 2 µm. See Supp. Movie 3.

I. Cytoplasmic Securin^{IFY-1} levels were measured throughout meiosis I and the mean ± s.e.m is shown in the graph.

Bel Borja et al. Figure 2

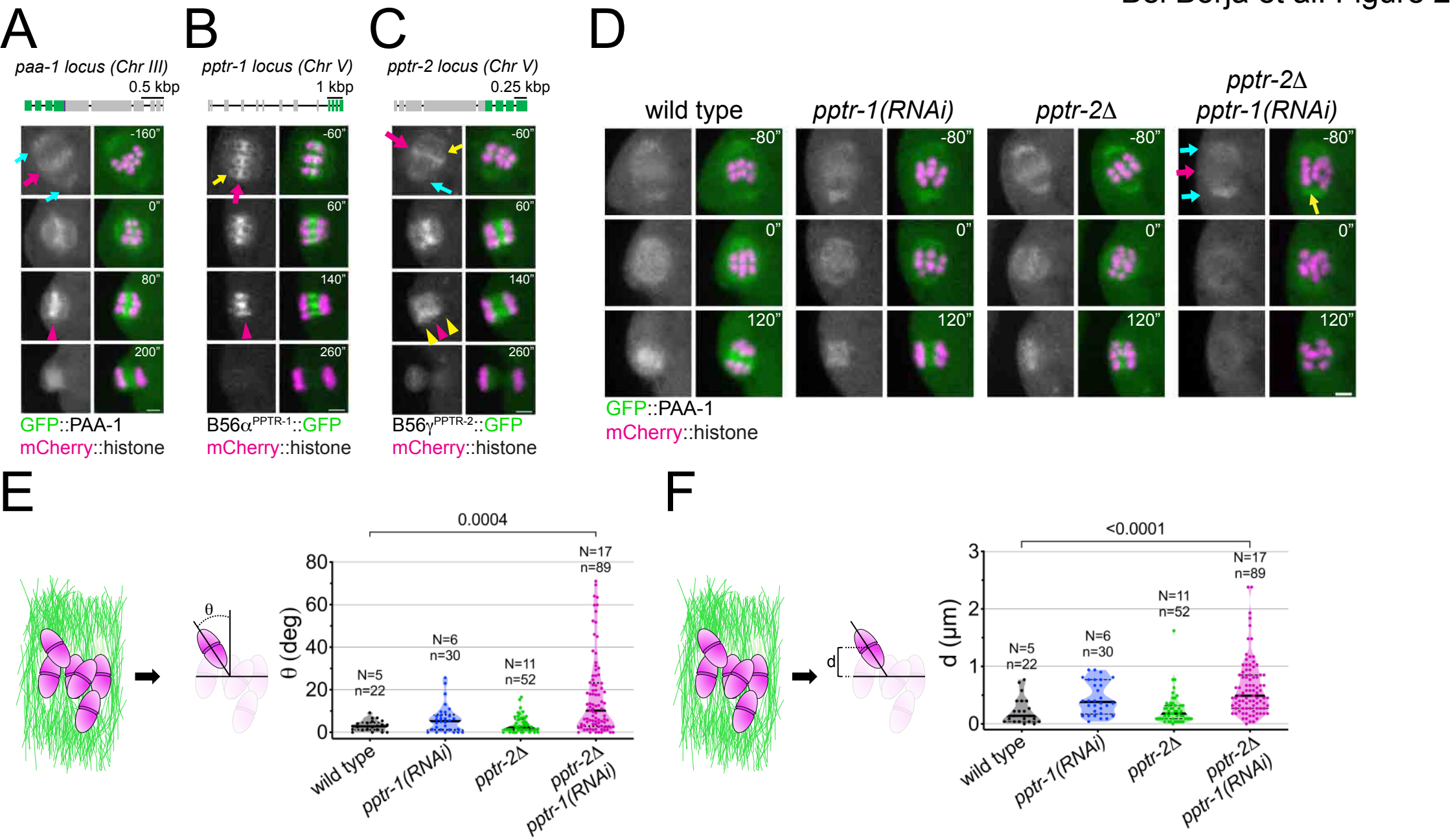

Figure 2. *C. elegans* B56 regulatory subunits PPTR-1 and PPTR-2 are required for normal Meiosis I.

A. Top**,** Schematic of the *paa-1* gene structure and its tagging with *gfp*. Bottom, the PP2A scaffold subunit GFP::PAA-1 was followed throughout meiosis I in a dissected oocyte. Magenta arrows point to the midbivalent; cyan arrows point to spindle poles and magenta arrowhead highlights the central-spindle localisation. Inset numbers represent the time relative to metaphaseI in seconds. Scale bar, 2 µm. See Supp. Movie 5.

B. Top, Schematic of the *pptr-1* gene structure and its tagging with *gfp*. Bottom, PPTR-1 and chromosome dynamics were followed in oocytes expressing PPTR-1::GFP and mCherry::histone. The magenta arrow points to the midbivalent and the yellow arrow points to the kinetochore. Magenta arrowhead highlights the central-spindle localisation. Inset numbers represent the time relative to metaphaseI in seconds. Scale bar, 2 µm. See Supp. Movie 6.

C. Top, Schematic of the *pptr-2* gene structure and its tagging with *gfp*. Bottom, PPTR-2 and chromosome dynamics were followed in oocytes expressing PPTR-2::GFP and mCherry::histone. The magenta arrow points to the midbivalent, the yellow arrow points to the kinetochore, and the cyan arrow to the spindle pole. Inset numbers represent the time relative to metaphaseI in seconds. Scale bar, 2 µm. Magenta arrowhead highlights the central-spindle localisation and yellow arrowhead highlights the chromosome-associated signal. See Supp. Movie 7.

D. PAA-1 and chromosome dynamics were followed in wild type, *pptr-1(RNAi)*, *pptr-2Δ,* and *pptr-2Δ+pptr-1(RNAi)* oocytes expressing GFP::PAA-1 and mCherry::histone. Magenta arrows point to the absence of GFP signal on prometaphase chromosomes and the cyan arrows point to spindle poles. The yellow arrows highlights one misaligned bivalent. Inset

numbers represent the time relative to metaphaseI in seconds. Scale bar, 2 µm. See Supp. Movie 8.

E. On the left, the schematic depicts how angles were measured relative to the spindle pole-to-pole axis. On the right, the angle of bivalents at 80 seconds before metaphase I in wild type, *pptr-1(RNAi)*, *pptr-2Δ* and *pptr-2Δ+pptr-1(RNAi)* oocytes. Violin plot includes each data point (chromosome), the median (straight black line), and the interquartile range (dashed black lines). N respresents number of oocytes and n number of bivalents measured. P values shown in the figure were obtained using a Kruskal-Wallis test.

F. On the left, the schematic depicts how distances were measured relative to the centre of the spindle. On the right, the distance of bivalents 80 seconds before metaphase I was measured in wild type, *pptr-1(RNAi)*, *pptr-2Δ* and *pptr-2Δ+pptr-1(RNAi)* oocytes. Violin plot includes each data point (chromosome), the median (straight black line), and the interquartile range (dashed black lines). N respresents number of oocytes and n number of bivalents measured. P values shown in the figure were obtained using a Kruskal-Wallis test.

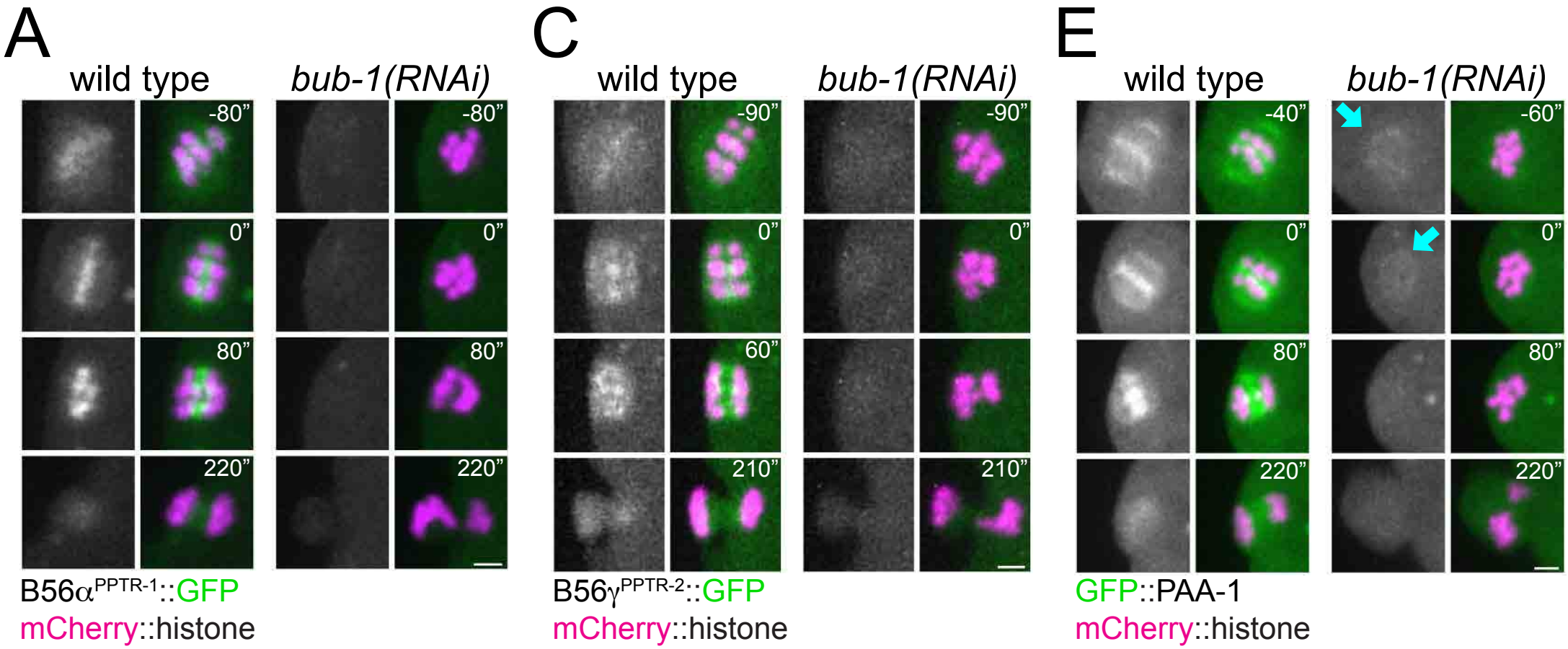
A
wild type
bub-1(RNAi)
-80”
0”
80”
220”
B56αPPTR-1::GFP
mCherry::histone
C
wild type
bub-1(RNAi)
-90”
0”
60”
210”
B56γPPTR-2::GFP
mCherry::histone
E
wild type
bub-1(RNAi)
-40”
-60”
0”
80”
220”
GFP::PAA-1
mCherry::histone

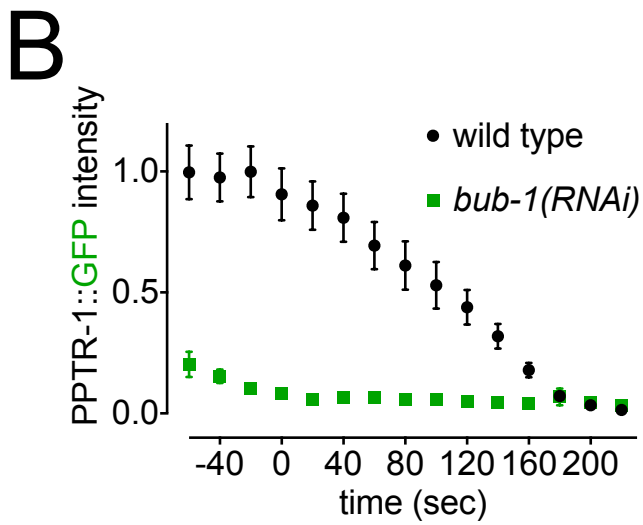
B
PPTR-1::GFP intensity
1.0
0.5
0.0
wild type
bub-1(RNAi)
-40 0 40 80 120 160 200
time (sec)

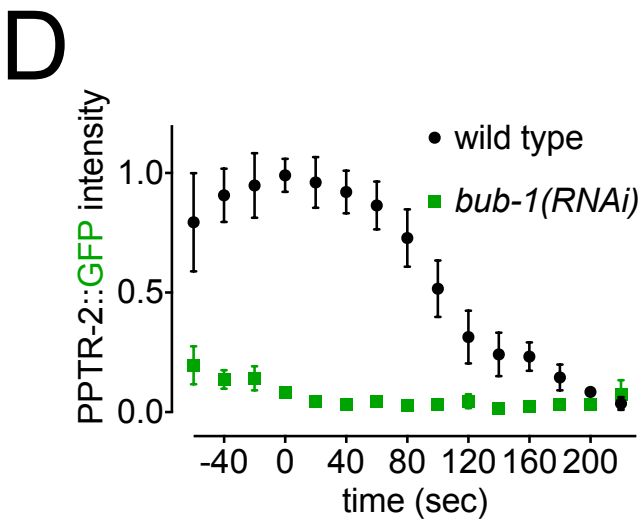
D
PPTR-2::GFP intensity
1.0
0.5
0.0
wild type
bub-1(RNAi)
-40 0 40 80 120 160 200
time (sec)

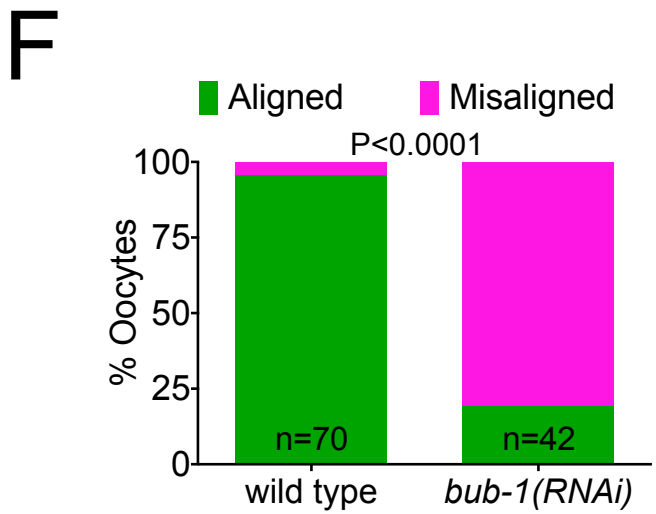
F
Aligned
Misaligned
P<0.0001
% Oocytes
100
75
50
25
0
n=70
n=42
wild type
bub-1(RNAi)

Figure 3. BUB-1 recruits B56α^{PPTR-1} and B56γ^{PPTR-2} during oocyte meiosis.

A. B56α^{PPTR-1} and chromosome dynamics were followed in wild type and *bub-1(RNAi)* oocytes expressing PPTR-1::GFP and mCherry::histone. Scale bar, 2 µm. See Supp. Movie 9.

B. PPTR-1::GFP levels were measured in wild type and *bub-1(RNAi)* oocytes throughout meiosis I and the mean ± s.e.m is shown in the graph.

C. B56γ^{PPTR-2} and chromosome dynamics were followed in wild type and *bub-1(RNAi)* oocytes expressing PPTR-2::GFP and mCherry::histone. Scale bar, 2 µm. See Supp. Movie 10.

D. PPTR-2::GFP levels were measured in wild type and *bub-1(RNAi)* oocytes throughout meiosis I and the mean ± s.e.m is shown in the graph.

E. Scaffold subunit PAA-1 and chromosome dynamics were followed in wild type and *bub-1(RNAi)* oocytes expressing GFP::PAA-1 and mCherry::histone. cyan arrows highlight the GFP::PAA-1 remaining in *bub-1(RNAi)* oocytes. Scale bar, 2 µm. See Supp. Movie 11.

F. The number of oocytes with misaligned chromosomes at metaphaseI in wild type and *bub-1(RNAi)* oocytes was analysed and the percentage is represented ($P<0.0001$, Fisher's exact test).

Bel Borja et al. Figure 4

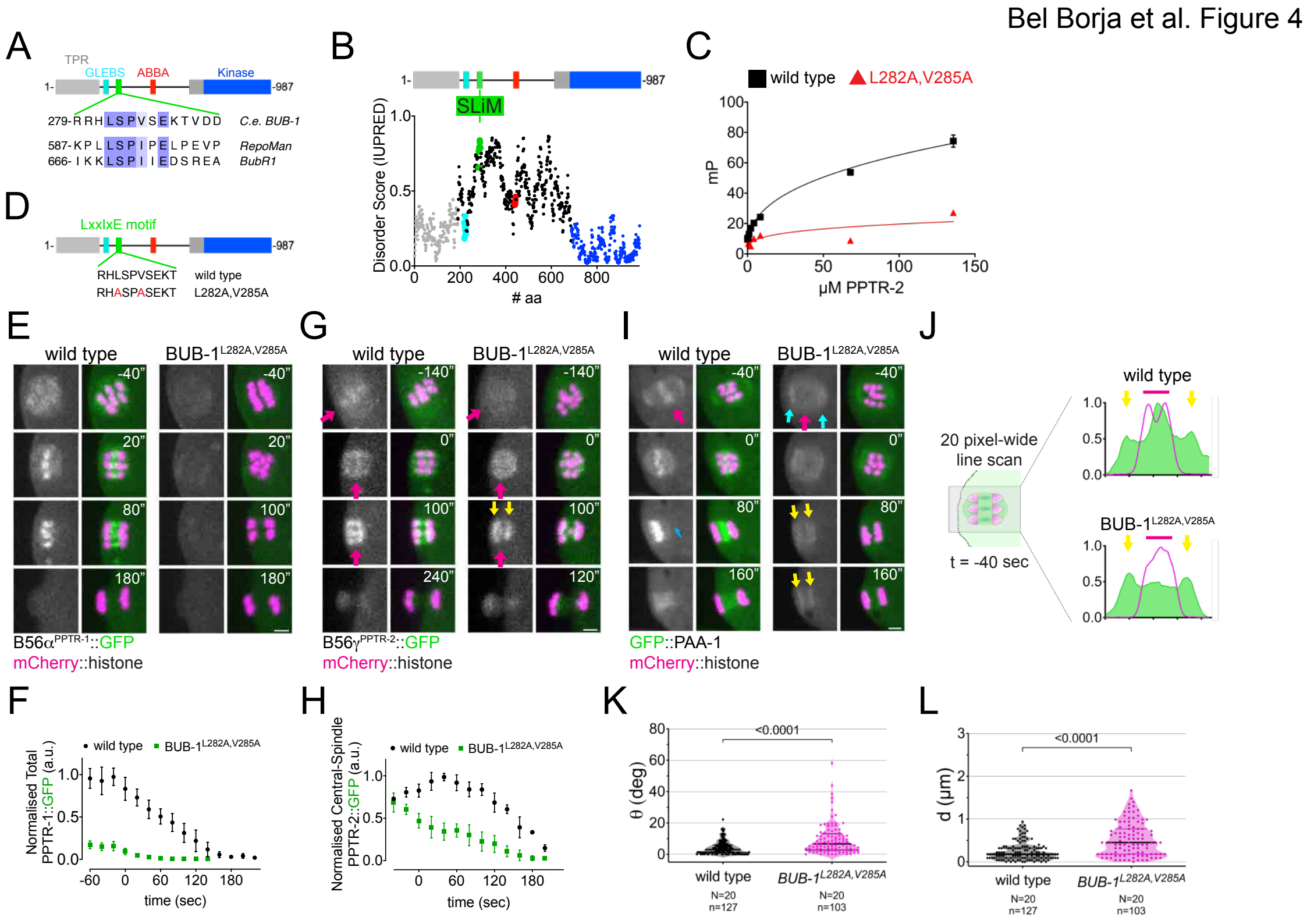

Figure 4. B56α^{PPTR-1} and B56γ^{PPTR-2} are targeted through a LxxIxE motif in BUB-1.

A. *C. elegans* BUB-1 LxxIxE SLiM is shown aligned with BubR1 and Repoman SLiMs. The only change within the LxxIxE sequence itself is the presence of a valine instead of isoleucine, which still fits within the consensus (Wang et al., 2016). The alignment was performed using Clustal Omega and visualised with Jalview (Waterhouse et al., 2009).

B. Disorder prediction of full-length BUB-1 was done using IUPRED2A (Erdős and Dosztányi, 2020). All prevuously characterised BUB-1 domains fall within ordered regions <0.5). The putative SLiM is in a disordered region (IUPRED score ~0.8).

C. PPTR-2 interaction with a LxxIxE motif-containing synthetic peptide was assessed using fluorescence polarisation. Increasing amounts of purified recombinant PPTR-2 were incubated with FITC-labelled wild type or L282A,V285A mutant peptide. The graph was taken from a representative experiment and shows the mean ± s.d. of technical triplicates.

D. Schematic showing the LxxIxE motif in BUB-1 and the BUB-1^{L282A,V285A} mutant.

E. B56α^{PPTR-1} and chromosome dynamics were followed in wild type and in BUB-1^{L282A,V285A} oocytes expressing PPTR-1::GFP and mCherry::histone. Scale bar, 2 µm. See Supp. Movie 13.

F. PPTR-1::GFP levels were measured in wild type and BUB-1^{L282A,V285A} oocytes throughout meiosis I and the mean ± s.e.m is shown in the graph.

G. B56γ^{PPTR-2} and chromosome dynamics were followed in wild type and in BUB-1^{L282A,V285A} oocytes expressing PPTR-2::GFP and mCherry::histone. Magenta arrows point towards prometaphase chromosomes and anaphase central-spindle whereas yellow arrows point towards the chromosome-associated anaphase signal. Scale bar, 2 µm. See Supp. Movie 14.

H. Midbivalent/Central spindle PPTR-2::GFP levels were measured in wild type and BUB-1^{L282A,V285A} oocytes throughout meiosis I and the mean ± s.e.m is shown in the graph.

I. GFP::PAA-1 is present on chromosomes in the BUB-1^{L282A,V285A} mutant. PAA-1 and chromosome dynamics were followed in wild type and in BUB-1^{L282A,V285A} oocytes expressing GFP::PAA-1 and mCherry::histone. Magenta arrows point towards prometaphase chromosomes and anaphase central-spindle whereas yellow arrows point towards the chromosome-associated anaphase signal. Cyan arrows point towards spindle poles. Scale bar, 2 µm. See Supp. Movie 15.

J. Representative, spindle-wide (20 pixels) line profiles are shown for wild type (top) and BUB-1^{L282A,V285A} mutant (bottom) measured in prometaphase I (40 seconds before metaphase I). Green arrows point to the PAA-1 pole signal and blue line to the chromosome associated population.

K. The angle of bivalents 80 seconds before segregation in meiosis I relative to the average angle of the spindle was measured in wild type and in BUB-1^{L282A,V285A} oocytes. Violin plot includes each data point (chromosome), the median (straight black line), and the interquartile range (dashed black lines). N respresents number of oocytes and n number of bivalents measured. P value shown in the figure was obtained using a Mann-Whitney test.

L. Distance of bivalents 80 seconds before segregation in meiosis I relative to the center of the spindle was measured in wild type and in BUB-1^{L282A,V285A} oocytes. Violin plot includes each data point (chromosome), the median (straight black line), and the interquartile range (dashed black lines). N respresents number of oocytes and n number of bivalents measured. P value shown in the figure was obtained using a Mann-Whitney test.

Bel Borja et al. Figure 5

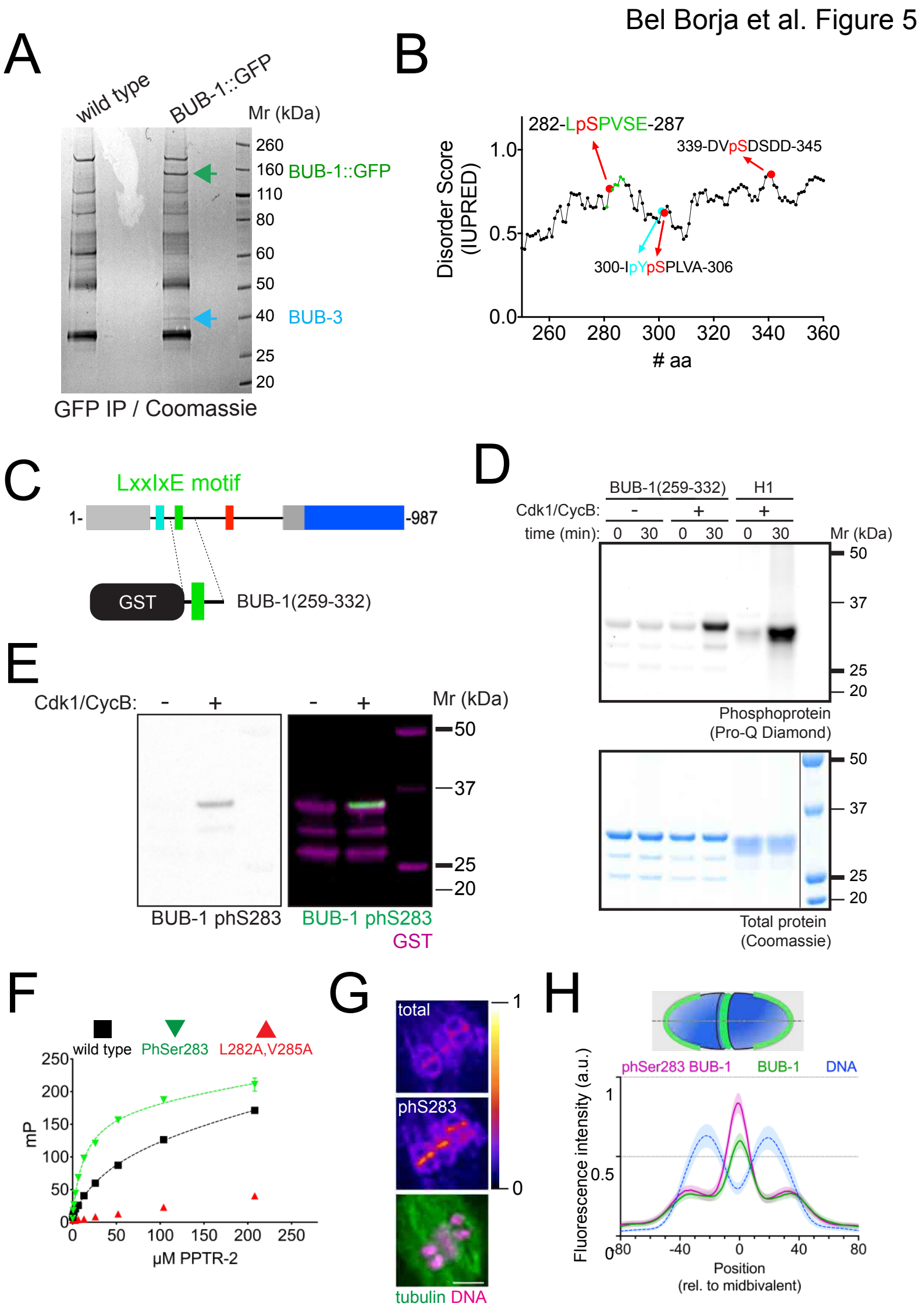

Figure 5. Phosphorylation of Ser 283 within the LxxIxE motif regulates B56 subunit binding.

A. BUB-1::GFP was immunoprecipitated and the eluted proteins were run on SDS-PAGE followed by coomassie staining. The position of BUB-1::GFP and BUB-3 are highlighted with green and blue arrows, respectively. The band corresponding to BUB-1::GFP was further analysed by mass spectrometry to look for phospho-modified peptides.

B. Serine 283 is phosphorylated in vivo. In addition, three other phosphorylation sites were identified within this disordered region.

C. A fragment of BUB-1 (259-332) containing the LxxIxE motif (282-287) was expressed in bacteria fused to a GST tag.

D. GST-BUB-1(259-332) was phosphorylated in vitro using Cdk1/CyclinB ('Cdk1/CycB'). Histone H1 was used as a positive control. Reactions were run on 4-12% SDS-PAGE and subject to phosphoprotein staining (top) followed by total protein staining (bottom).

E. GST-BUB-1(259-332) was phosphorylated in vitro using Cdk1/CyclinB ('Cdk1/CycB') and subject to western blotting using a specific antibody against phosphorylated Serine 283. Anti-GST served as a loading control for the substrate.

F. PPTR-2 interaction with a LxxIxE motif-containing synthetic peptide was assessed using fluorescence polarisation. Increasing amounts of purified recombinant PPTR-2 were incubated with FITC-labelled wild type, Serine 283 phosphorylated, or L282A,V285A mutant peptide. The graph was taken from a representative experiment and shows the mean ± s.d. of technical triplicates.

G. Fixed oocytes were subject to immunofluorescence using labelled BUB-1 ('total'), phospho-Ser283-BUB-1 ('phS283'), and tubulin. Single-channel images for BUB-1 and phospho-Ser283-BUB-1 are shown in 'fire' LUT and the bottom panel shows tubulin (green) and DNA (magenta).

H. Line profile analysis was performed in samples co stained with labelled BUB-1 (Alexa488) and phospho-Ser283-BUB-1 (Alexa647) as described in the methods section. The lines represent the mean and the shaded area represents the s.d. of the indicated number of bivalents.

Bel Borja et al. Figure 6

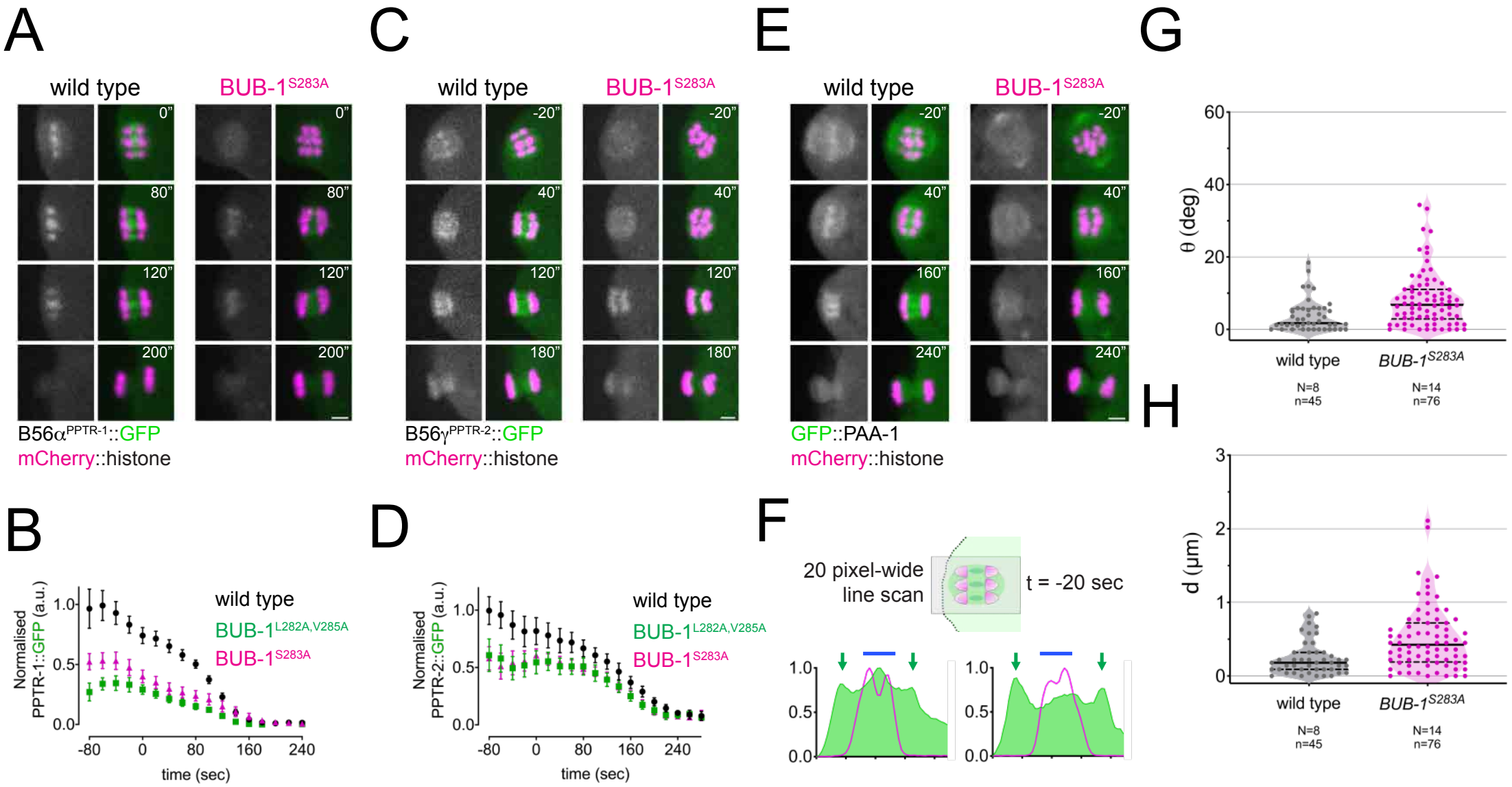

Figure 6. LxxIxE motif phosphorylation regulates the recruitment of B56s subunits in vivo.

A. B56α^{PPTR-1} and chromosome dynamics were followed in wild type and in BUB-1^{S283A} oocytes expressing PPTR-1::GFP and mCherry::histone. Scale bar, 2 µm. See Supp. Movie 16.

B. PPTR-1::GFP levels were measured in wild type, BUB-1^{L282A,V285A} and in BUB-1^{S283A} oocytes throughout meiosis I and the mean ± s.e.m. is shown in the graph.

C. B56γ^{PPTR-2} and chromosome dynamics were followed in wild type and in BUB-1^{S283A} oocytes expressing PPTR-2::GFP and mCherry::histone. Scale bar, 2 µm. See Supp. Movie 17.

D. PPTR-2::GFP levels were measured in wild type, BUB-1^{L282A,V285A} and in BUB-1^{S283A} oocytes throughout meiosis I and the mean ± s.e.m is shown in the graph.

E. GFP::PAA-1 is present on chromosomes in the BUB-1^{S283A} mutant. PAA-1 and chromosome dynamics were followed in wild type and in BUB-1^{S283A} oocytes expressing GFP::PAA-1 and mCherry::histone. Yellow dotted line shows that chromosome associated PAA-1 is lost in the BUB-1^{S283A} mutant. Scale bar, 2 µm. See Supp. Movie 18.

F. Representative, spindle-wide (20 pixels) line profiles are shown for wild type (left) and BUB-1^{S283A} mutant (right) measured in prometaphase I (20 seconds before metaphase I). Green arrows point to the PAA-1 pole signal and blue line to the chromosome associated population.

G. Angle of bivalents 80 seconds before segregation in meiosis I relative to the average angle of the spindle was measured in wild type and in BUB-1^{S283A} oocytes. Violin plot includes each data point (chromosome), the median (straight black line), and the interquartile range (dashed black lines). N respresents number of oocytes and n number of bivalents measured. P value shown in the figure was obtained using a Mann-Whitney test.

I. Distance of bivalents 80 seconds before segregation in meiosis I relative to the center of the spindle was measured in wild type and in BUB-1^{S283A} oocytes. Violin plot includes each data point (chromosome), the median (straight black line), and the interquartile range (dashed black lines). N respresents number of oocytes and n number of bivalents measured. P value shown in the figure was obtained using a Mann-Whitney test.

Bel Borja et al. Figure 7

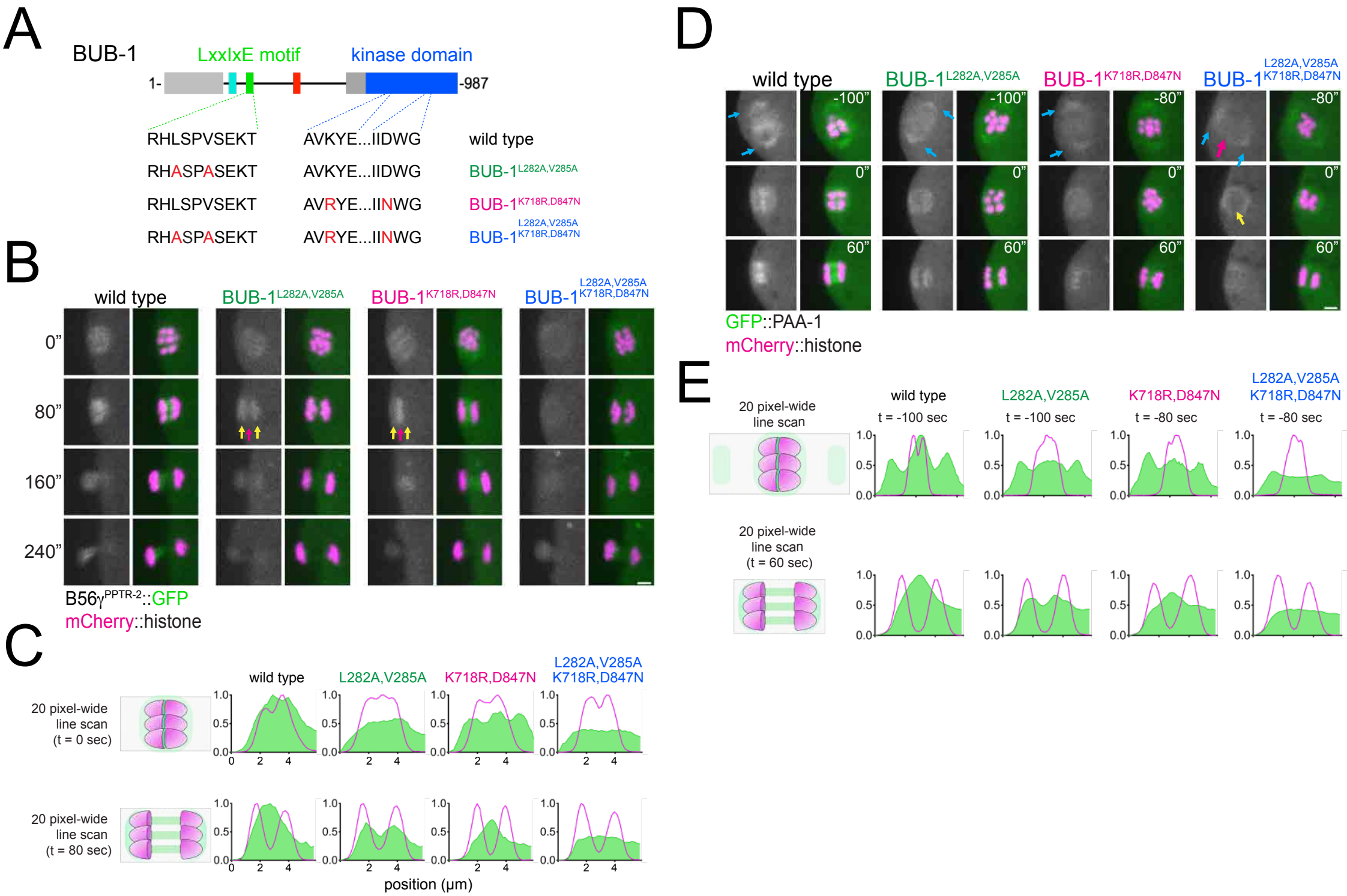

Figure 7. Role of BUB-1 kinase domain in B56γ^{PPTR-2} chromosomal targeting

A. Schematic showing the LxxIxE motif and the kinase domain in BUB-1 of the wild type, the BUB-1^{L282A,V285A}, BUB-1^{K718R,D847N}, and BUB-1$^{L282A,V285A,\ K718R,D847N}$ mutant.

B. B56γ^{PPTR-2} and chromosome dynamics were followed in wild type, the BUB-1^{L282A,V285A}, BUB-1^{K718R,D847N}, and BUB-1$^{L282A,V285A,\ K718R,D847N}$ oocytes expressing PPTR-2::GFP and mCherry::histone. Magenta arrows point towards the central spindle and yellow arrows towards chromosomes. Scale bar, 2 µm. See also Supp. Movie 20.

C. Representative, spindle-wide (20 pixels) line profiles are shown for wild type, the BUB-1^{L282A,V285A}, BUB-1^{K718R,D847N}, and BUB-1$^{L282A,V285A,\ K718R,D847N}$. On top profiles of metaphase plate just in anaphase onset, on the bottom profiles 80 seconds after segregation to show central spindle levels.

D. Scaffolding subunit PAA-1 and chromosome dynamics were followed in wild type, the BUB-1^{L282A,V285A}, BUB-1^{K718R,D847N}, and BUB-1$^{L282A,V285A,\ K718R,D847N}$ oocytes expressing GFP::PAA-1 and mCherry::histone. Cyan arrows point to pole population of PAA-1, magenta arrow signals chromosomes, and yellow arrow highlight the levels of PAA-1 in anaphase onset. Scale bar, 2 µm. See also Supp. Movie 21.

E. Representative, spindle-wide (20 pixels) line profiles are shown for wild type, the BUB-1^{L282A,V285A}, BUB-1^{K718R,D847N}, and BUB-1$^{L282A,V285A,\ K718R,D847N}$. On top profiles before segregation starts (different time points matching the first pannel on Figure 7D) to highlight the PAA-1 in the poles, on the bottom profiles 60 seconds after segregation to show central spindle levels.

	PPTR-1	B56β1	B56ε3	B56α2	PPTR-2	B56δ3	B56γ1
PPTR-1		60.12	71.87	68.30	52.26	60.17	64.48
PPTR-2	52.26	56.36	63.94	60.84		66.19	68.97

Table 1. Sequence identity between full-length mammalian B56 isoforms and *C.elegans* orthologues PPTR-1 and PPTR-2. Table was created using Clustal Omega version 2.1. See Supplementary Table 1 for full Percent Identity Matrix.

Bel Borja et al. Supp. Figure 1

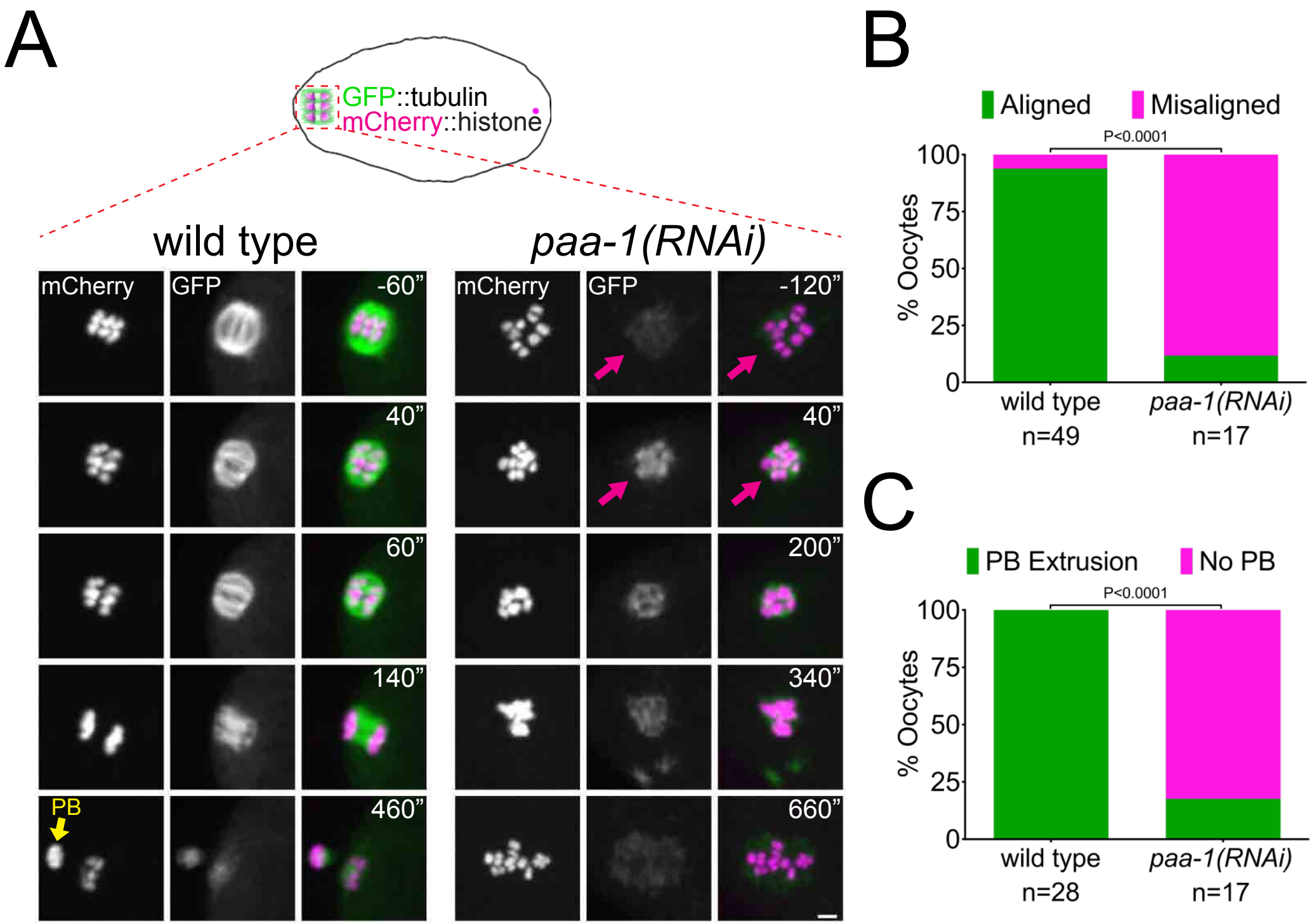

Supplementary Figure 1. PP2A is essential for Meiosis I in *C. elegans* oocytes.

A. Microtubule and chromosome dynamics were followed in wild type and *paa-1(RNAi)* oocytes expressing GFP::tubulin and mCherry::histone. Yellow arrow shows polar body (PB) and magenta arrows point to the lack of a bipolar spindle in *paa-1(RNAi)* oocytes. Inset numbers represent the time relative to metaphase I in seconds. Scale bar, 2 µm.

B. The number of oocytes with misaligned chromosomes at metaphase I in wild type and *paa-1(RNAi)* oocytes was analysed and the percentage is represented ($P<0.0001$, Fisher's exact test).

C. The number of oocytes with an extruded polar body (PB) after meiosis I in wild type and *paa-1(RNAi)* oocytes was analysed and the percentage is represented ($P<0.0001$, Fisher's exact test).

Bel Borja et al. Supp. Figure 2

A

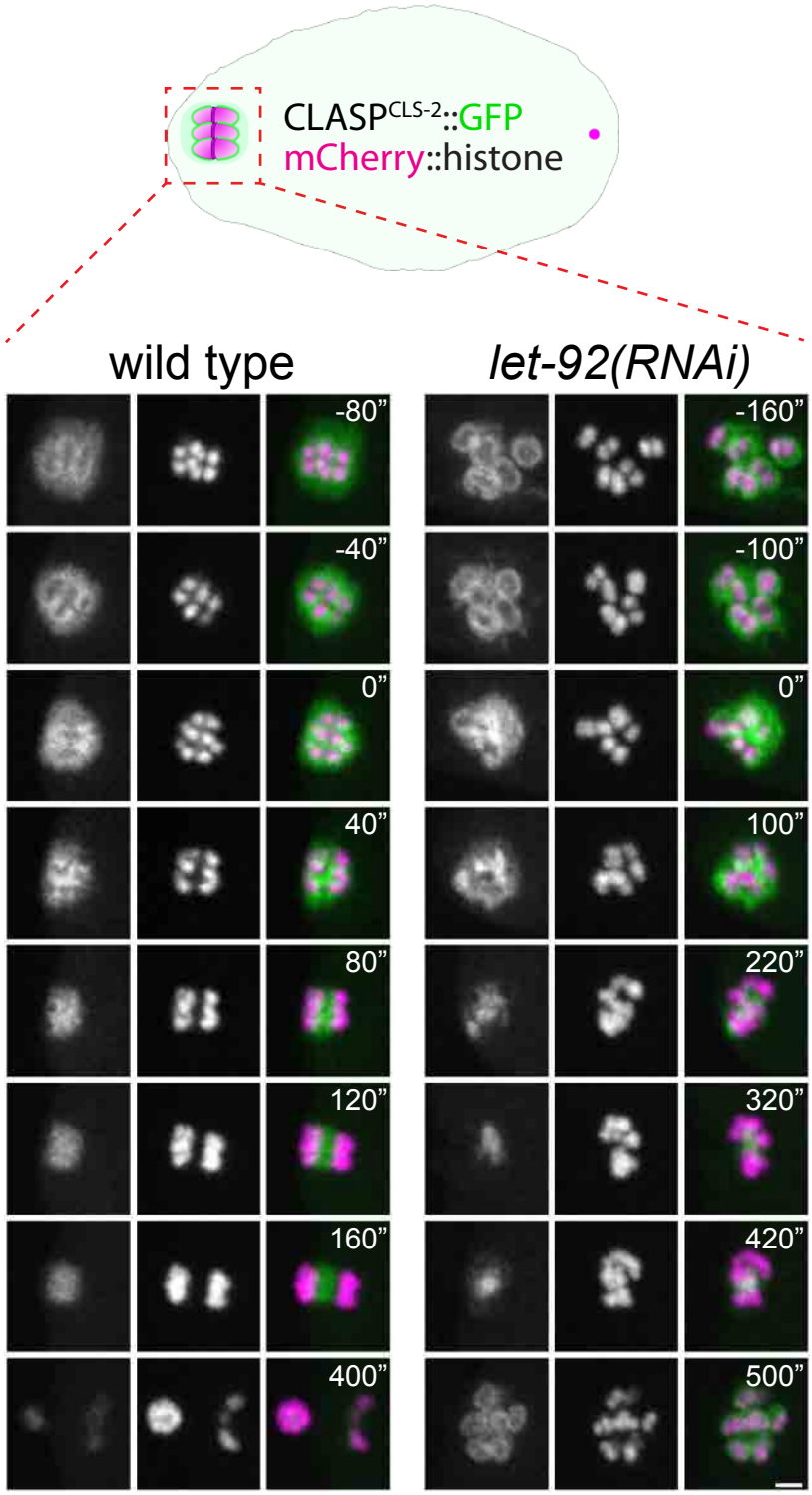

B

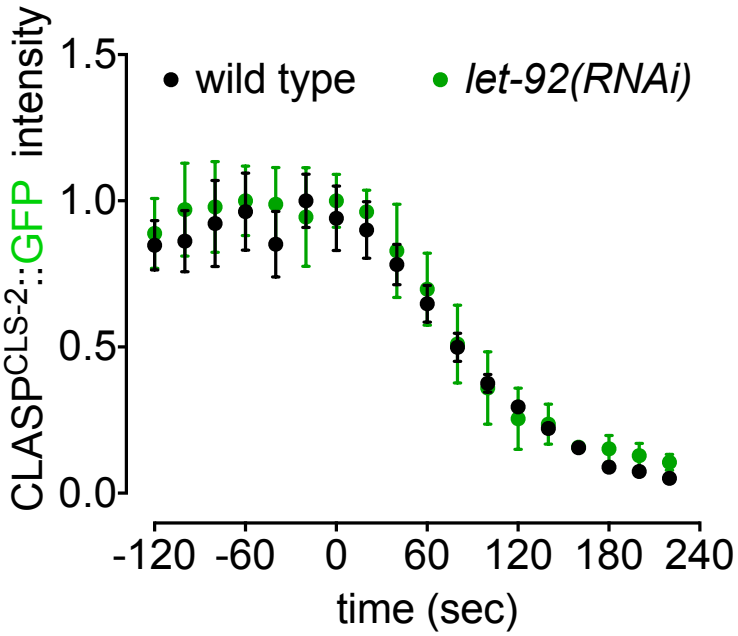

Supplementary Figure 2. CLASP^{CLS-2} intensity and localization is not affected after let-92 depletion.

A. CLASP^{CLS-2} and chromosome dynamics were followed in wild type and *let-92(RNAi)* oocytes expressing CLASP^{CLS-2}::GFP and mCherry::histone. Inset numbers represent the time relative to metaphase I in seconds. Scale bar, 2 µm. See Supp. Movie 4.

B. CLASP^{CLS-2}::GFP levels were measured throughout meiosis I in wild type and *let-92(RNAi)* and the mean ± s.e.m is shown in the graph.

Bel Borja et al. Supp. Figure 3

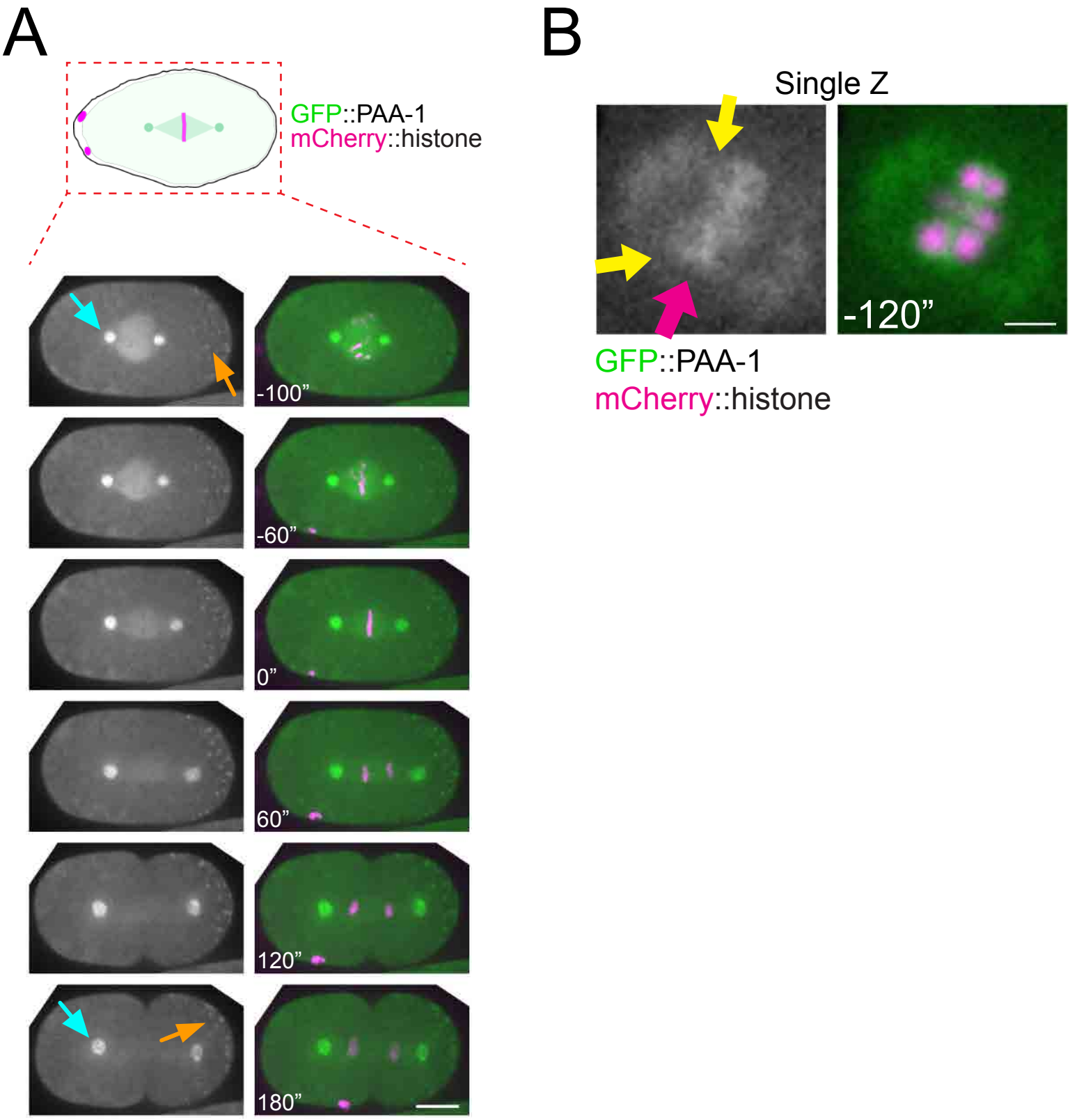

Supplementary Figure 3. Localisation of GFP::PAA-1 during mitosis.

A. PAA-1 localisation was followed during the first mitotic division using endogenously tagged GFP::PAA-1. Cyan arrows point to centrosomes and orange arrows point to P-bodies. Inset numbers represent the time relative to metaphase in seconds. Scale bar, 10 µm.

B. A single Z plane from one time-point (-120") from the same movie as in Figure 2A is shown to highlight that the chromosomal PAA-1 signal is a combination of midbivalent (magenta arrow) and kinetochore (yellow arrows).

Bel Borja et al. Supp. Figure 4

A

Regulatory (B) Subunit	
human	*C. elegans*
PPP2R2A / B55α	SUR-6
PPP2R2B / B55β	
PPP2R2C / B55γ	
PPP2R2D / B55δ	
PPP2R5C / B56γ	PPTR-2
PPP2R5D / B56δ	
PPP2R5A / B56α	PPTR-1
PPP2R5E / B56ε	
PPP2R5B / B56β	

B

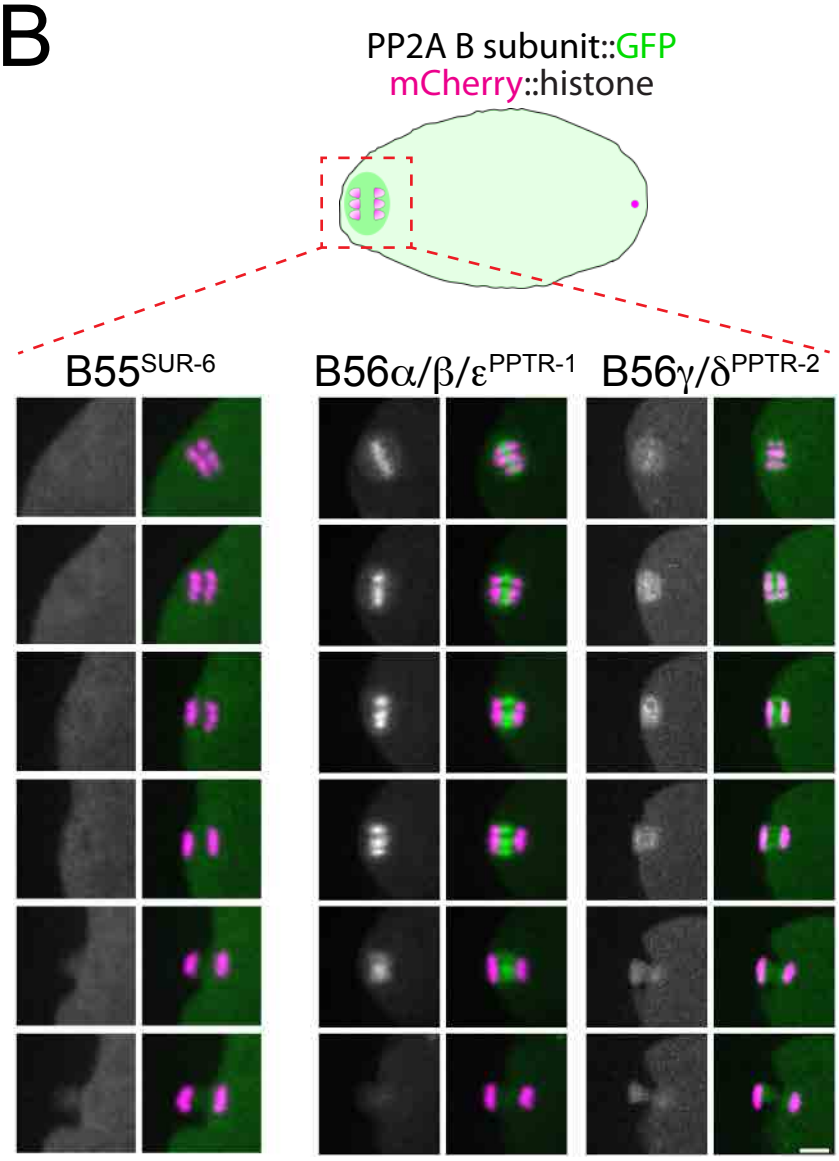

C

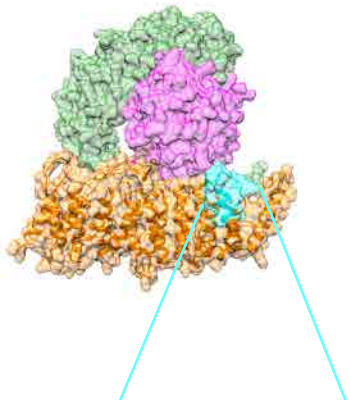

```
B56γ     378- SKTHWNKTIHGLIYNA -393
B56δ     454- SKSHWNKTIHGLIYNA -469
PPTR-2   449- SKSHWNKTIHGLIYNA -464
B56β     409- SKEHWNQTIVSLIYNV -424
PPTR-1   420- SKEHWNQTIVALVYNV -435
B56α     403- SKEHWNPTIVALVYNV -418
B56ε     395- SKEHWNPAIVALVYNV -410
              ** *** :* .*:**.
```

Supplementary Figure 4. Localisation of *C. elegans* B55 and B56 subunits.

A. Chart showing the *C. elegans* orthologues of the human B55 and B56 regulatory B subunits. The chart is based on the alignment provided in Table 1 and Supplementary Table 1.

B. The respective B subunit was endogenously tagged with GFP and their localisation was followed by imaging of dissected oocytes. Scale bar, 2 µm.

C. Alignment of the human and *C. elegans* B56 subunits in the C-terminal stretch shown to be important for kinetochore vs centromere localisation of B56 in human cells during mitosis (Vallardi et al. 2019).

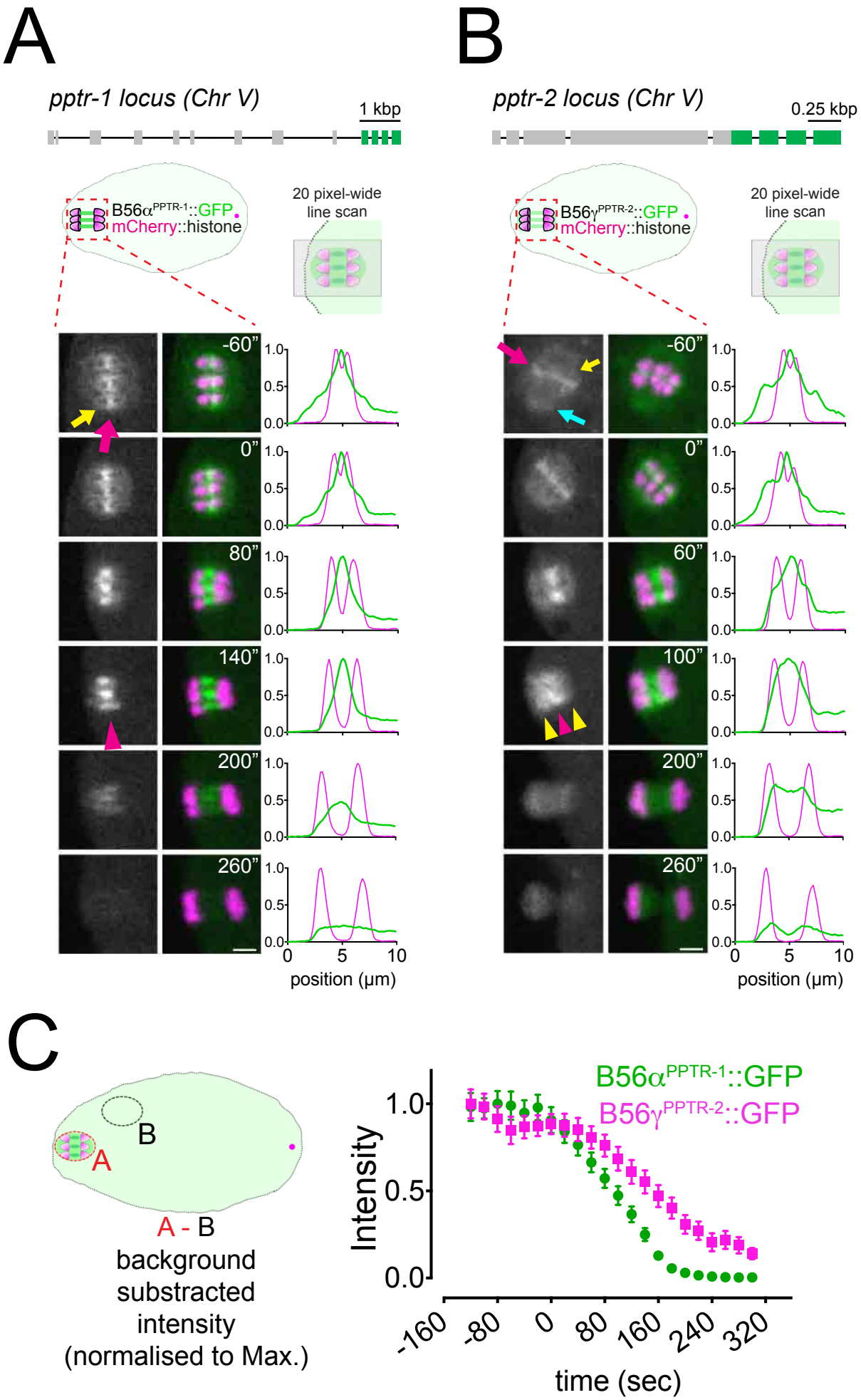
A
pptr-1 locus (Chr V)
1 kbp
B56α^PPTR-1::GFP
mCherry::histone
20 pixel-wide line scan
-60"
0"
80"
140"
200"
260"
1.0
0.5
0.0
0
5
10
position (µm)
B
pptr-2 locus (Chr V)
0.25 kbp
B56γ^PPTR-2::GFP
mCherry::histone
20 pixel-wide line scan
-60"
0"
60"
100"
200"
260"
position (µm)
C
B
A
A - B
background substracted intensity (normalised to Max.)
B56α^PPTR-1::GFP
B56γ^PPTR-2::GFP
Intensity
1.0
0.5
0.0
-160
-80
0
80
160
240
320
time (sec)

Supplementary Figure 5. Localisation of *C. elegans* B55 and B56 subunits.

A. Top, Schematic of the *pptr-1* gene structure and its tagging with *gfp*. Bottom, PPTR-1 and chromosome dynamics were followed in oocytes expressing PPTR-1::GFP and mCherry::histone. The magenta arrow points to the midbivalent and the yellow arrow points to the kinetochore. Magenta arrowhead highlights the central-spindle localisation. Inset numbers represent the time relative to metaphaseI in seconds. Scale bar, 2 µm. Representative, spindle-wide (20 pixels) line profiles are shown on the right of each time point. See Supp. Movie 6.

B. Top, Schematic of the *pptr-2* gene structure and its tagging with *gfp*. Bottom, PPTR-2 and chromosome dynamics were followed in oocytes expressing PPTR-2::GFP and mCherry::histone. The magenta arrow points to the midbivalent, the yellow arrow points to the kinetochore, and the cyan arrow to the spindle pole. Inset numbers represent the time relative to metaphaseI in seconds. Scale bar, 2 µm. Magenta arrowhead highlights the central-spindle localisation and yellow arrowhead highlights the chromosome-associated signal. Representative, spindle-wide (20 pixels) line profiles are shown on the right of each time point. See Supp. Movie 7.

C. PPTR-1::GFP and PPTR-2::GFP levels were measured throughout meiosis I and the mean ± s.e.m is shown in the graph.

Bel Borja et al. Supp. Figure 6

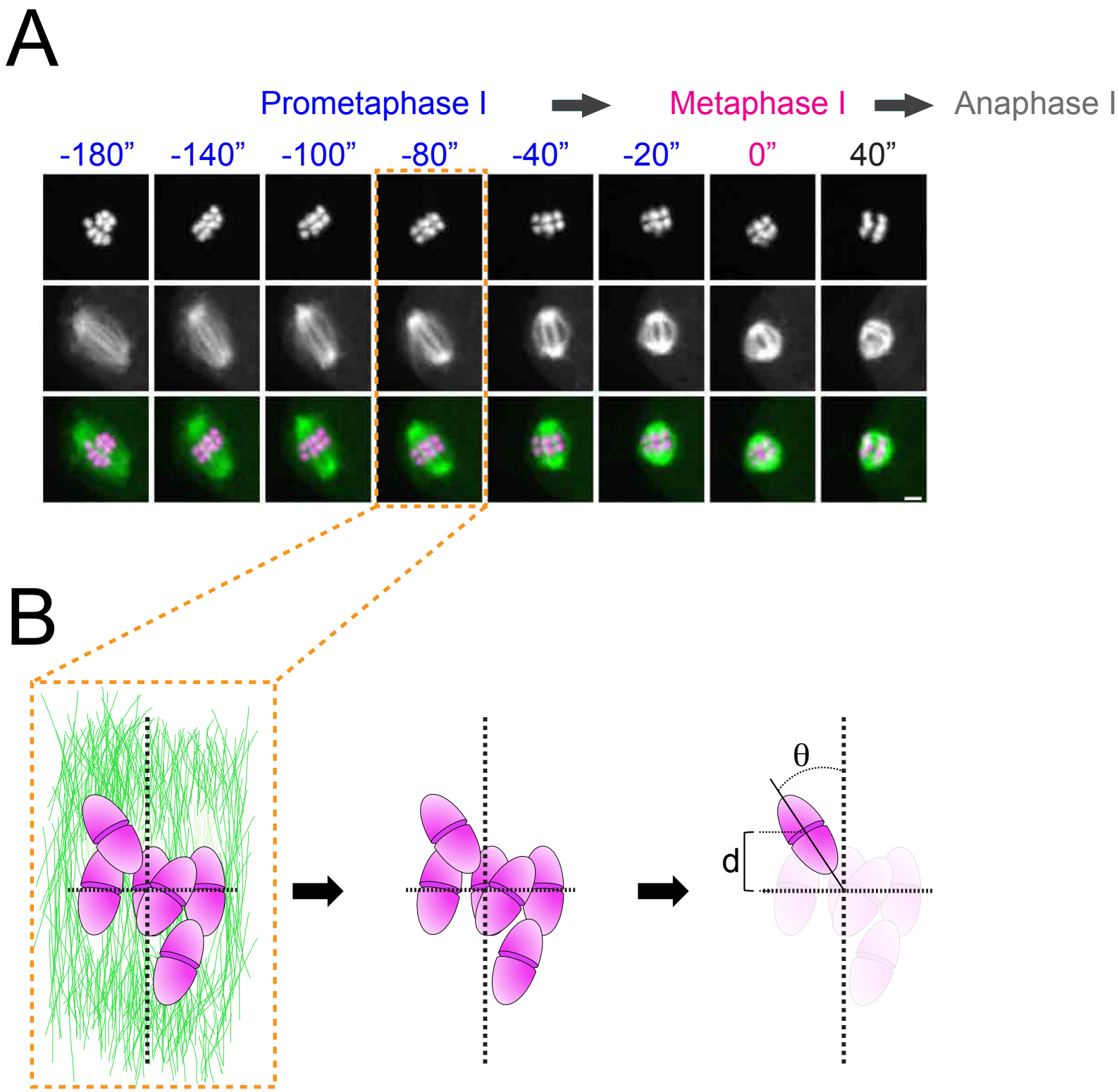

Supplementary Figure 6. Schematics of how congression and alignment were anotated in this study.

A. Microtubules and chromosomes of a wild type oocyte are shown in the panel. For the congression/alignment analysissuring prometaphase I, we chose to analyse 80 seconds before metaphase I, as chromosome are readily aligned in most wild type oocytes.

B. Schematic of a prometaphase I spindle indicating how the angle and the distance of each bivalent was measured.

Bel Borja et al. Supp. Figure 7

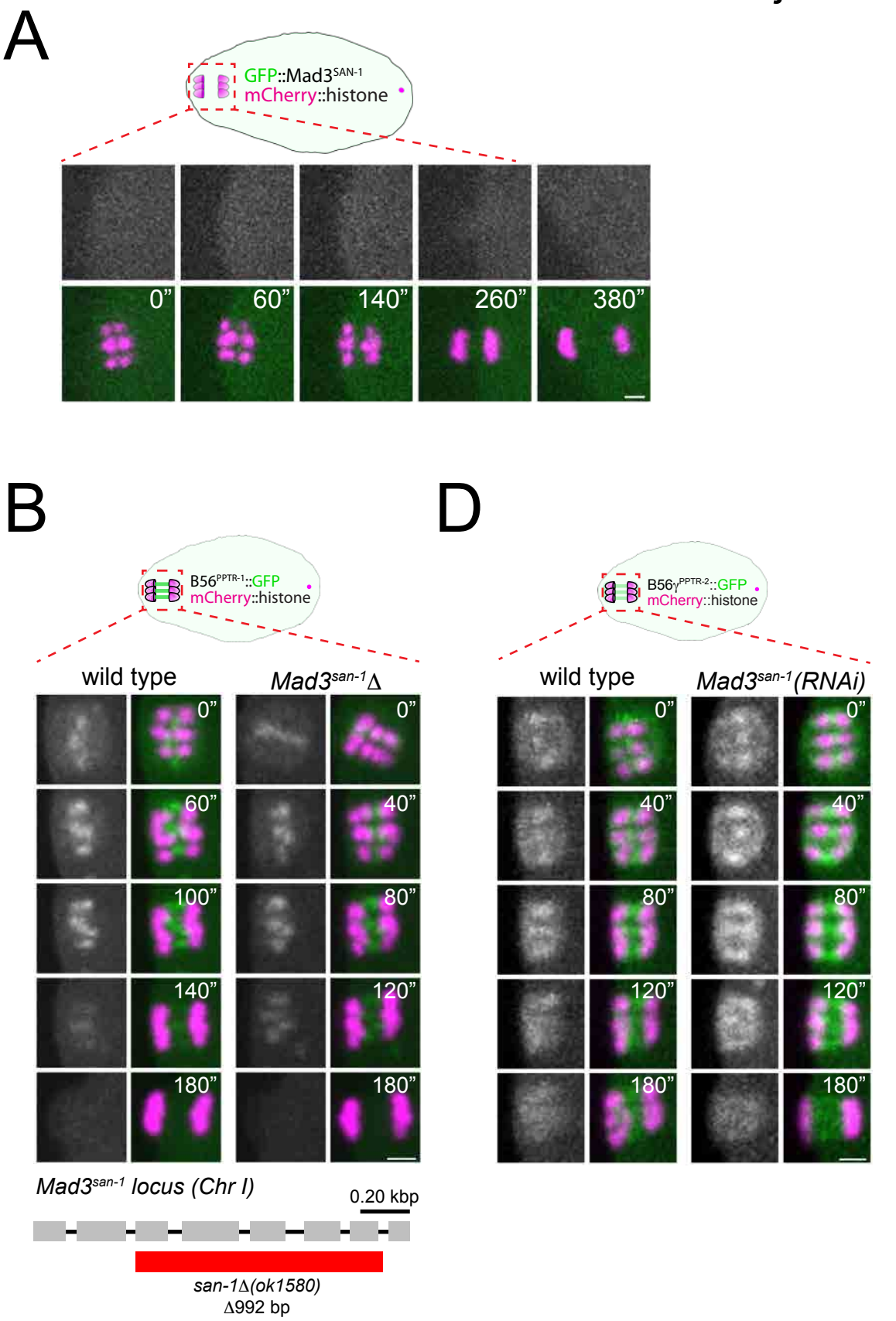

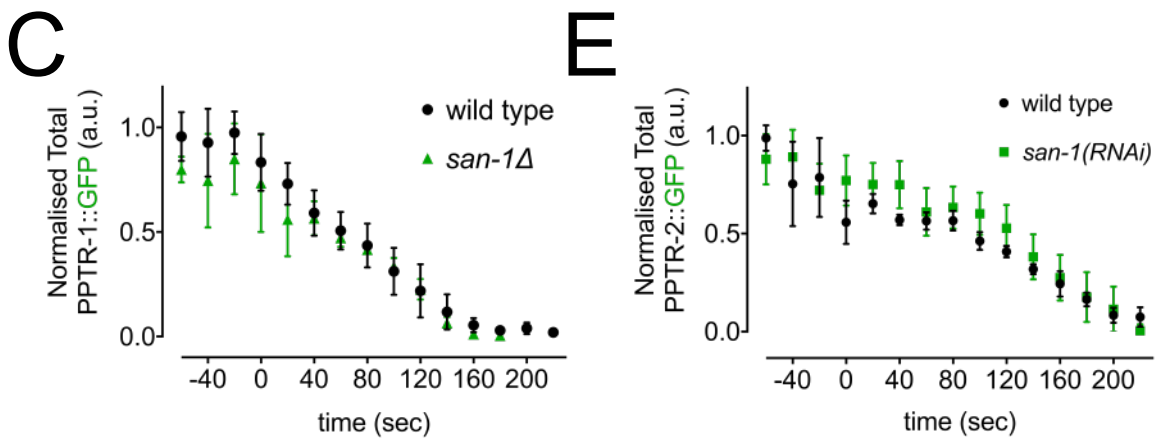

Supplementary Figure 7. Mad3^{SAN-1} does not play a major role in B56α^{PPTR-1} and B56γ^{PPTR-2} targeting.

A. GFP::Mad3^{SAN-1} was imaged during oocyte meiosis along with mCherry::histone to follow chromosomes. Time insets are relative to metaphase I ('t=0'). Scale bar, 2 µm.

B. B56α^{PPTR-1} and chromosome dynamics were followed in wild type and in *Mad3^{SAN-1}Δ* oocytes expressing PPTR-1::GFP and mCherry::histone. Scale bar, 2 µm. The bottom panel shows a schematic of the *san-1Δ* allele.

C. B56γ^{PPTR-2} and chromosome dynamics were followed in wild type and in *Mad3^{san-1}(RNAi)* oocytes expressing PPTR-2::GFP and mCherry::histone. Scale bar, 2 µm.

Bel Borja et al. Supp. Figure 8

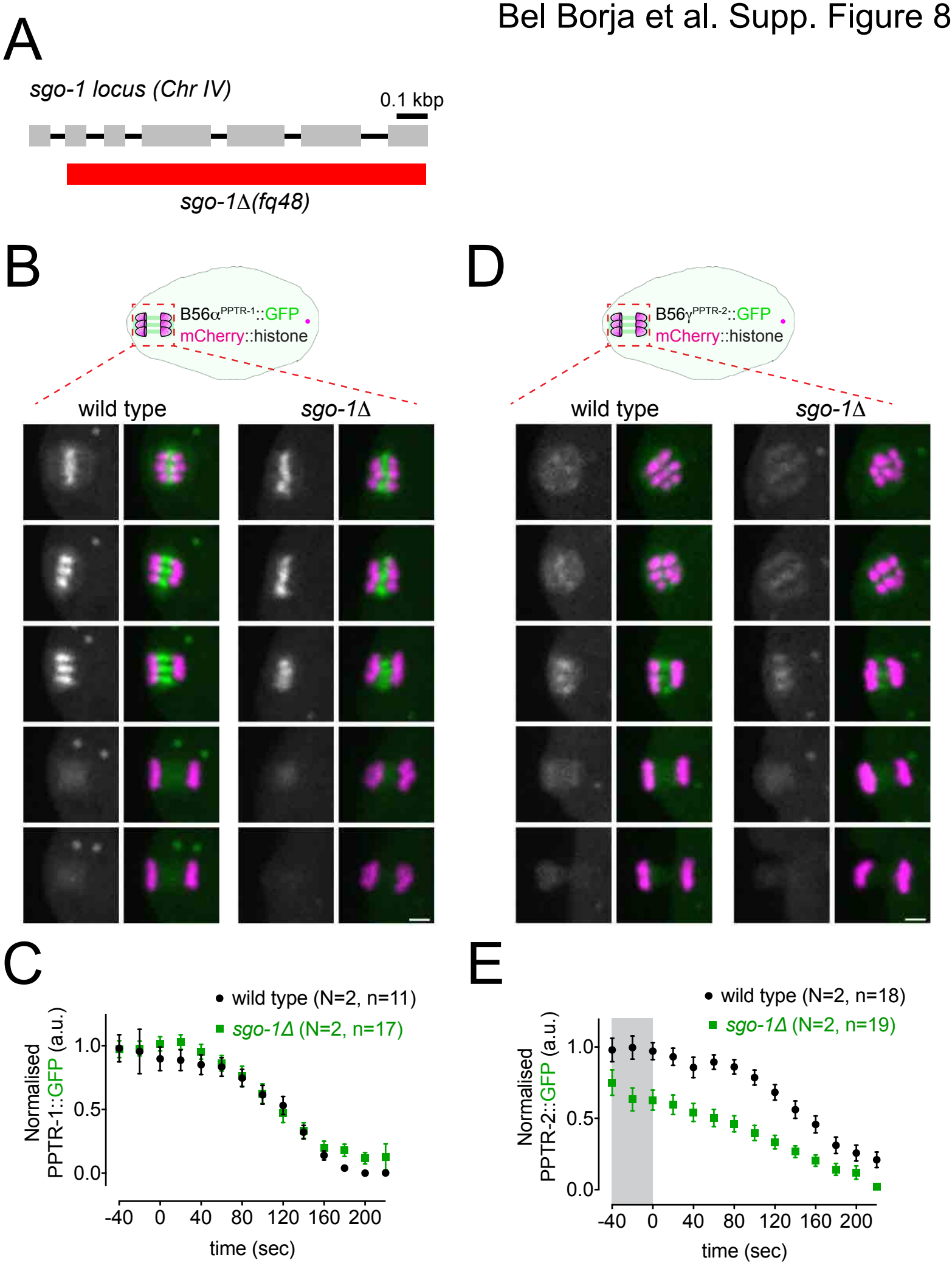

Supplementary Figure 8. Shugoshin^{SGO-1} does not play a major role in B56α^{PPTR-1} and B56γ^{PPTR-2} targeting.

A. Schematic of the *sgo-1Δ* allele.

B. B56α^{PPTR-1} and chromosome dynamics were followed in wild type and in *Shugoshin^{sgo-1}*oocytes expressing PPTR-1::GFP and mCherry::histone. Scale bar, 2 µm.

C. PPTR-1::GFP levels were measured in wild type and in *Shugoshin^{sgo-1}*oocytes throughout meiosis I and the mean ± s.e.m is shown in the graph. N represents number of experiments and n number of oocytes quantified.

D. B56γ^{PPTR-2} and chromosome dynamics were followed in wild type and *Shugoshin^{sgo-1}*oocytes expressing PPTR-2::GFP and mCherry::histone. Scale bar, 2 µm.

E. PPTR-1::GFP levels were measured in wild type and in *Shugoshin^{sgo-1}*oocytes throughout meiosis I and the mean ± s.e.m is shown in the graph. N represents number of experiments and n number of oocytes quantified.

Bel Borja et al. Supp. Figure 9

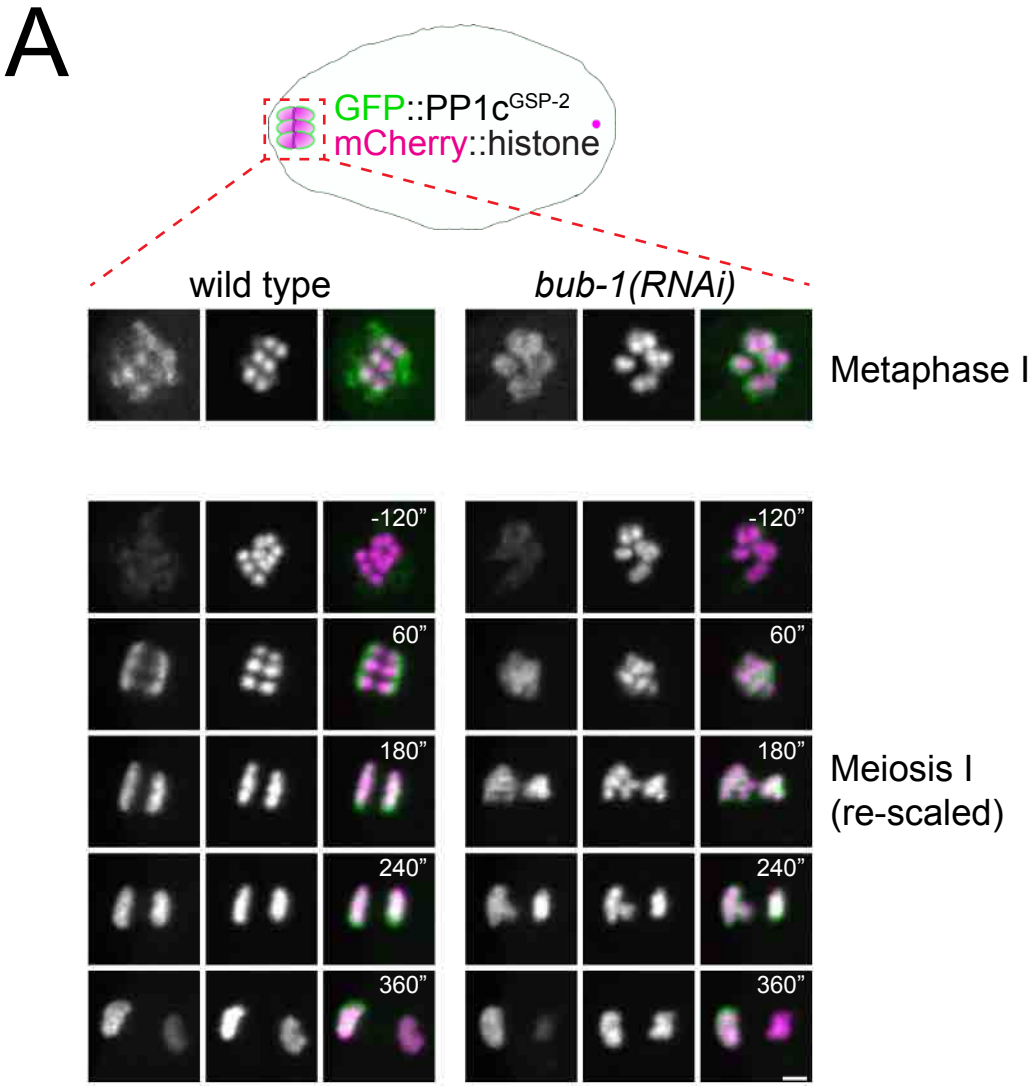

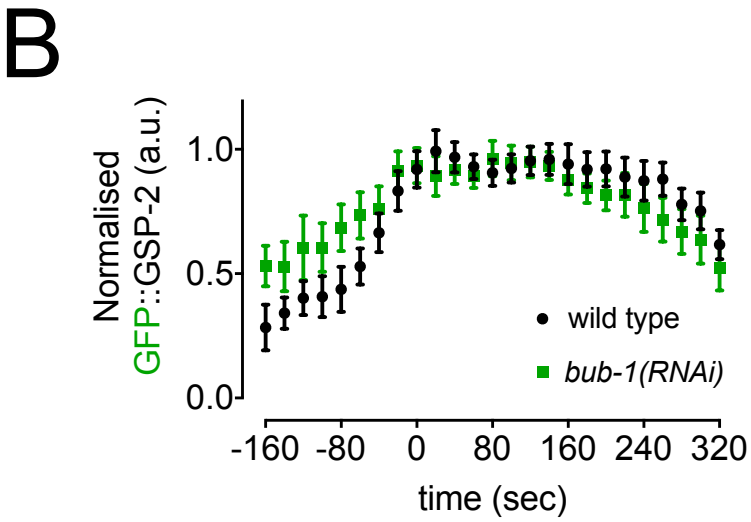

Supplementary Figure 9. PP1 catalytic subunit localisation is not regulated by BUB-1.

A. GFP::PP1c^{GSP-2} and chromosome dynamics were followed in wild type and *bub-1(RNAi)* oocytes. Since the GFP signal increases during anaphase, one scale was chosen to show kinetochore localisation during metaphase I (top) and another for the composite panel (bottom). Scale bar, 2 µm. See Supp. Movie 12.

B. GFP::PP1c^{GSP-2} levels were measured in wild type and *bub-1(RNAi)* oocytes throughout meiosis I and the mean ± s.e.m is shown in the graph.

Bel Borja et al. Supp. Figure 10

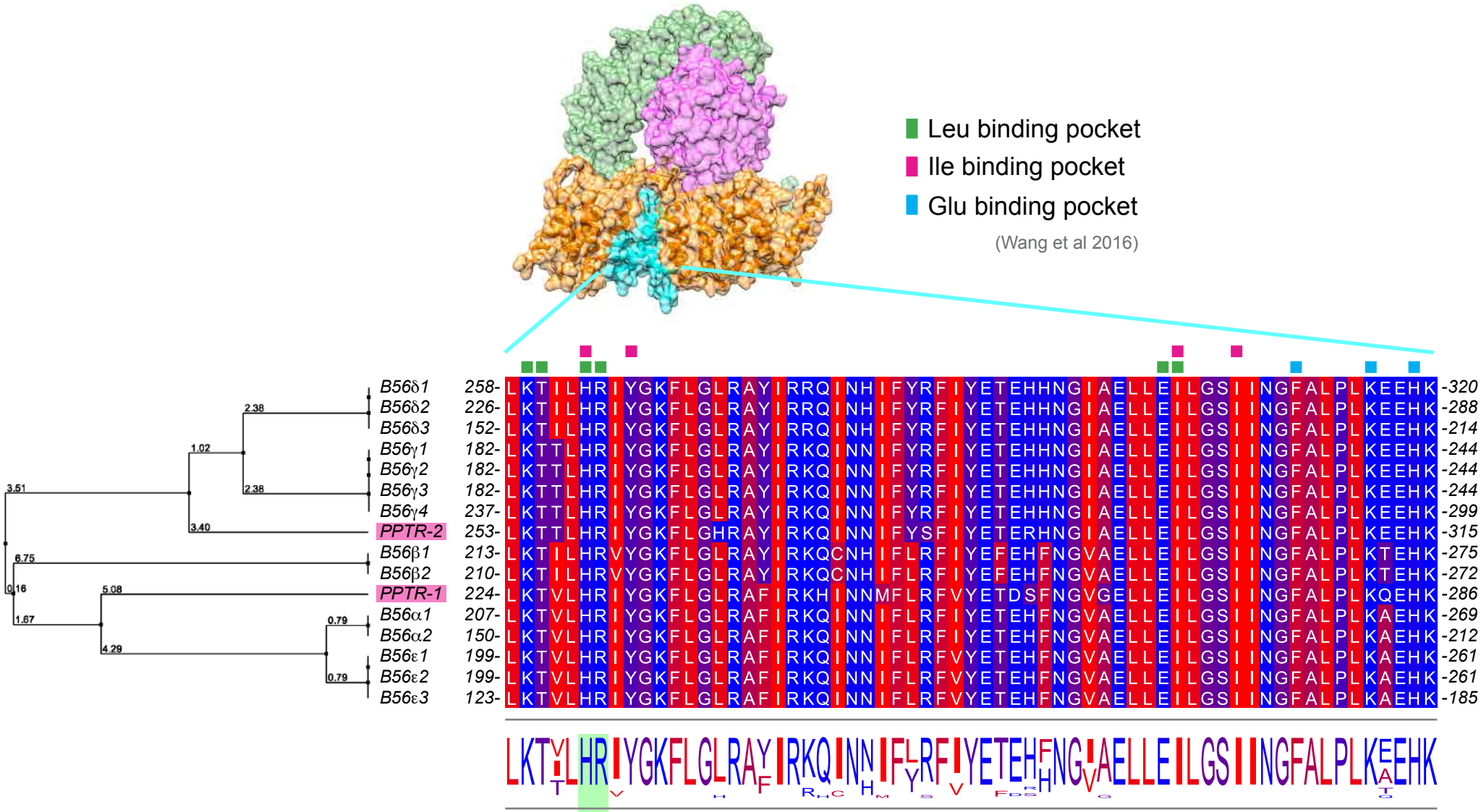

R188 (B56γ1) salt bridge with phS (SLiM)

H187 (B56γ1) H-bond with phS carbonyl (SLiM)

Supplementary Figure 10. Alignment of the B56 subunits LxxIxE motif binding pocket. *C. elegans* and human B56 subunits LxxIxE motif binding pocket were aligned using Clustal Omega and Jalview. The scale from blue to red represents increasing hydrophobicity. Key residues as reported in Wang et al. (2016) are highlighted. Additionally, residues making contact with the phospho-serine are highlighted with green background. The tree on the left was calculated from the distance matrix generated from sequence pairwise scores and confirms the relationship between *C. elegans* and human B56s.

Bel Borja et al. Supp. Figure 11

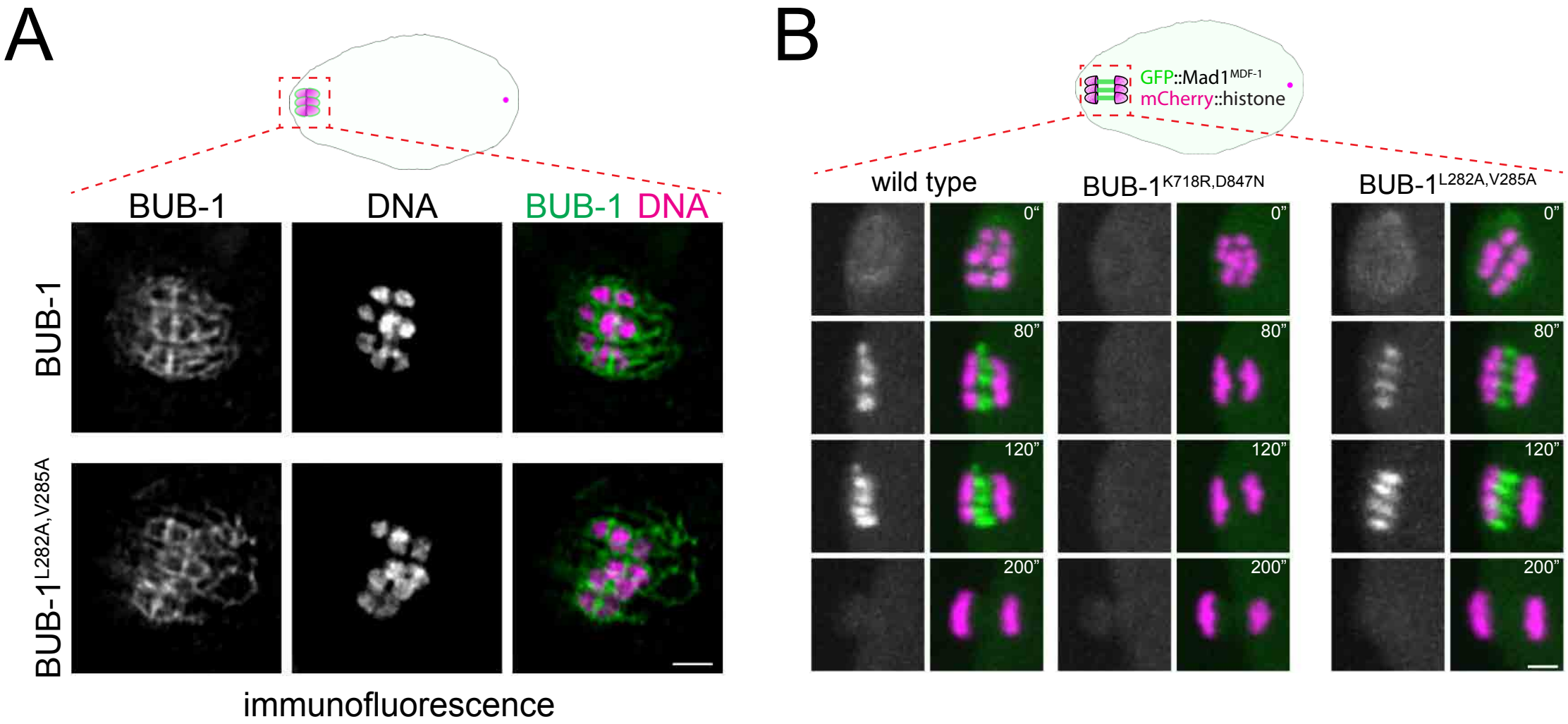

Supplementary Figure 11. Mad1^{MDF-1} localisation is not affected by a LxxIxE motif mutation in BUB-1.

A. BUB-1 localisation was analysed in fixed wild type and BUB-1^{L282A,V285A} mutant oocytes by immunofluorescence using BUB-1 specific antibodies. Scale bar, 2 µm.

B. GFP::Mad1^{MDF-1} was imaged during oocyte meiosis along with mCherry::histone to follow chromosomes. Time insets are relative to metaphase I (t=0”). The BUB-1^{K718R,D847N} mutation completely abolishes Mad1^{MDF-1} localisation. On the other hand, GFP::Mad1^{MDF-1} remained unaltered in the the BUB-1^{L282A,V285A} mutant. Scale bar, 2 µm.

A

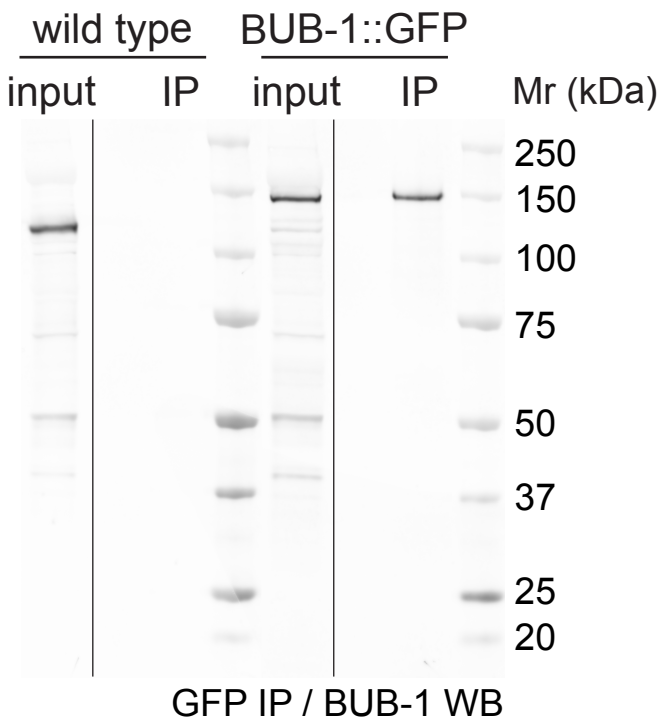

B

R.HLphSPVSEK.T

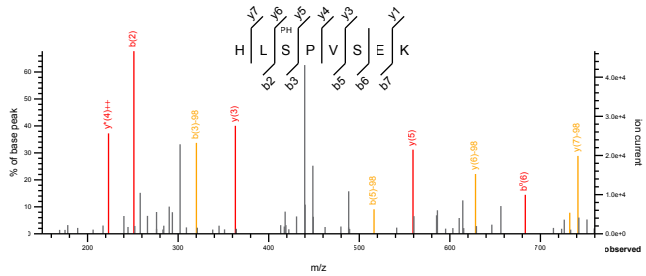

R.RHLphSPVSEK.T

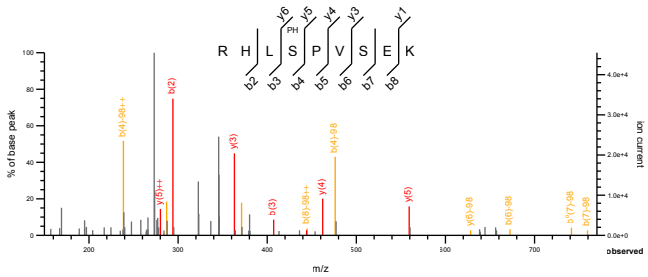

R.RRHLphSPVSEK.T

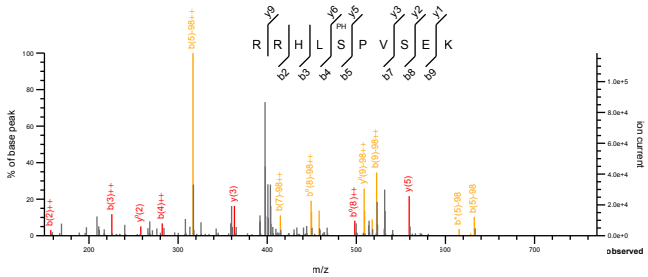

Supplementary Figure 12. BUB-1::GFP immunoprecipitation and selected MS spectra of peptides containing phospho serine 283.

A. Embryo extracts from wild type (N2) and BUB-1::GFP worms were immunoprecipitated using a GFP nanobody coupled to magnetic beads. The inputs and immunoprecipitates were resolved on SDS-PAGE and subject to BUB-1 western blot. BUB-1::GFP is readily pulled down form the extracts, whereas untagged BUB-1 is not. Note the size difference due to the GFP tag. MW marker is shown on the right side.

B. Seleted MS spectra without (top), with one (middle), or with two (bottom) trypsin miscleavages are shown.

A

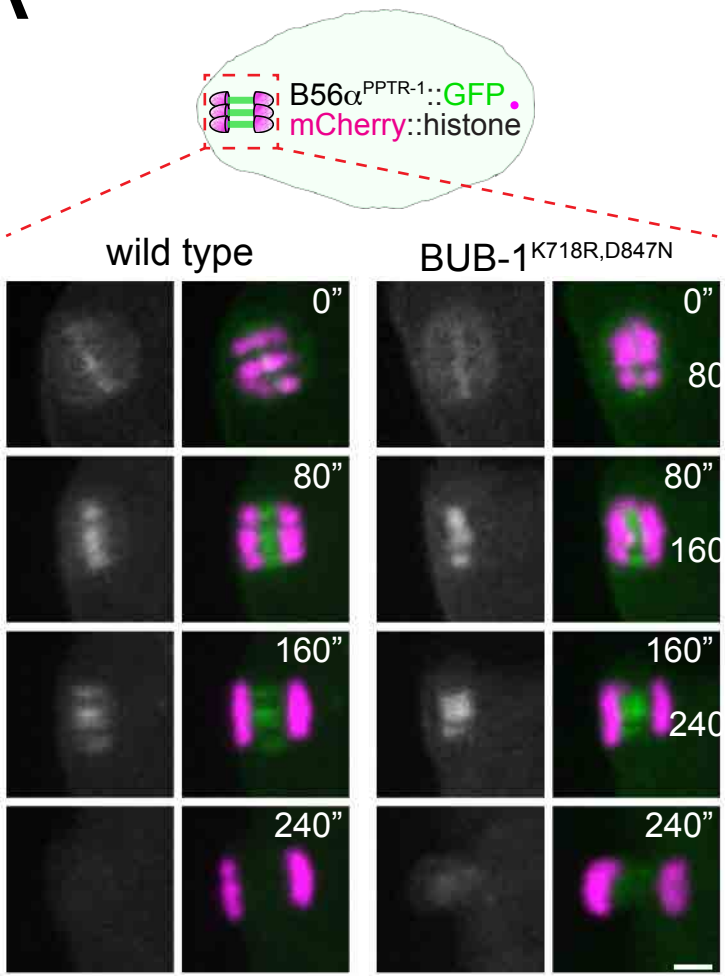
B56α^{PPTR-1}::GFP
mCherry::histone
wild type
BUB-1^{K718R,D847N}
0”
80”
160”
240”

B

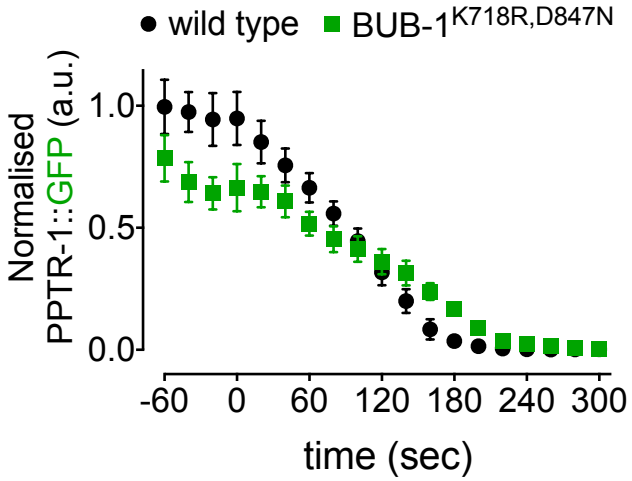
wild type
BUB-1^{K718R,D847N}
Normalised PPTR-1::GFP (a.u.)
1.0
0.5
0.0
-60
0
60
120
180
240
300
time (sec)

Supplementary Figure 13. Kinase domain in BUB-1 does not regulate targeting of B56α^{PPTR-1} regulatory subunit in meiosis I.

A. PPTR-1 and chromosome dynamics were followed in wild type and BUB-1^{K718R,D847N} oocytes expressing PPTR-1::GFP and mCherry::histone. Inset numbers represent the time relative to metaphaseI in seconds. Scale bar, 2 µm. See Supp. Movie 19.

B. PPTR-1::GFP levels were measured throughout meiosis I in wild type and BUB-1^{K718R,D847N} oocytes and the mean ± s.e.m is shown in the graph.

	PPTR-1	B56β1	B56β2	B56ε2	B56ε3	B56ε1	B56α2	B56α1	PPTR-2	B56δ1	B56δ2	B56δ3	B56γ4	B56γ5	B56γ1	B56γ2	B56γ3
PPTR-1		60.12	60.08	66.67	71.87	66.59	68.30	63.35	52.26	54.81	56.10	60.17	60.42	57.75	64.48	63.27	59.27
B56β1	60.12		97.56	72.17	73.66	71.83	71.79	69.77	56.36	62.75	63.85	67.13	65.28	64.47	66.21	67.13	64.44
B56β2	60.08	97.56		71.86	73.66	71.52	71.79	69.28	56.59	62.53	63.62	67.13	64.78	63.97	65.68	66.59	63.94
B56ε2	66.67	72.17	71.86		99.74	99.78	78.21	77.49	59.87	66.16	67.60	70.49	67.62	67.81	69.14	69.88	68.75
B56ε3	71.87	73.66	73.66	99.74			79.80	79.80	63.94	71.36	71.36	71.36	73.70	72.38	72.82	73.70	72.38
B56ε1	66.59	71.83	71.52	99.78			78.23	77.52	59.66	65.88	67.28	70.12	67.10	67.27	68.58	69.30	68.19
B56α2	68.30	71.79	71.79	78.21	79.80	78.23		99.07	60.84	67.92	69.14	69.14	71.53	69.56	70.74	71.78	69.79
B56α1	63.35	69.77	69.28	77.49	79.80	77.52	99.07		56.49	63.35	64.97	68.00	66.74	66.37	68.35	69.30	67.49
PPTR-2	52.26	56.36	56.59	59.87	63.94	59.66	60.84	56.49		62.31	61.76	66.19	63.55	60.66	68.97	66.25	62.74
B56δ1	54.81	62.75	62.53	66.16	71.36	65.88	67.92	63.35	62.31		99.65	98.19	79.07	75.68	81.29	80.00	76.72
B56δ2	56.10	63.85	63.62	67.60	71.36	67.28	69.14	64.97	61.76	99.65		98.39	79.72	77.37	82.46	81.05	77.63
B56δ3	60.17	67.13	67.13	70.49	71.36	70.12	69.14	68.00	66.19	98.19	98.39		84.40	81.72	87.62	85.71	81.72
B56γ4	60.42	65.28	64.78	67.62	73.70	67.10	71.53	66.74	63.55	79.07	79.72	84.40		94.57	93.00	93.81	93.61
B56γ5	57.75	64.47	63.97	67.81	72.38	67.27	69.56	66.37	60.66	75.68	77.37	81.72	94.57		92.87	94.64	95.23
B56γ1	64.48	66.21	65.68	69.14	72.82	68.58	70.74	68.35	68.97	81.29	82.46	87.62	93.00	92.87		99.77	98.44
B56γ2	63.27	67.13	66.59	69.88	73.70	69.30	71.78	69.30	66.25	80.00	81.05	85.71	93.81	94.64	99.77		99.79
B56γ3	59.27	64.44	63.94	68.75	72.38	68.19	69.79	67.49	62.74	76.72	77.63	81.72	93.61	95.23	98.44	99.79	

Supplementary Table 1. Percent Identity (%) Matrix of the full length sequence alignment of mammalian B56 isoforms and *C.elegans* orthologues PPTR-1 and PPTR-2 .Created with Clustal Omega version 2.1.

Markers / *mutants*	Strain Number	Genotype	Source
SUR-6::GFP	OD4579	*sur-6(ltl183[GFP::loxP::3xFlag::sur-6]) I*	this study
SUR-6::GFP; mCherry::histone	FGP354	*sur-6(ltl183[GFP::loxP::3xFlag::sur-6])I; ltIs37[pAA64; pie-1p::mCherry::his-58; unc-119 (+)]IV*	this study
GFP::tubulin; mCherry::histone	OD868	*ltSi220[pOD1249/pSW077; Pmex-5::GFP::tbb-2::operon_linker::mCHerry::his-11; cb-unc-119(+)]I*	Wang et al, 2015 (PMID: 24217623)
GFP::tubulin; mCherry::histone; *bub-1(L282A;V285A)*	FGP339	*ltSi220[pOD1249/pSW077; Pmex-5::GFP::tbb-2::operon_linker::mCHerry::his-11; cb-unc-119(+)]I; bub-1(syb1936[bub-1((L282A;V285A)])I*	this study
GFP::tubulin; mCherry::histone; *pptr-2 Δ*	FGP369	*pptr-2(ok1467)V; ltSi220[pOD1249/pSW077; Pmex-5::GFP::tbb-2::operon_linker::mCHerry::his-11; cb-unc-119(+)]I*	this study
GFP::tubulin; mCherry::histone; *bub-1(K718R;D847N)*	FGP337	*ltSi220[pOD1249/pSW077; Pmex-5::GFP::tbb-2::operon_linker::mCHerry::his-11; cb-unc-119(+)]I; bub-1(syb1746[bub-1((K718R;D847N)])*	this study
GFP::tubulin; mCherry::histone; bub-1(L282A;V285A;K718R;D847N)	FGP402	*ltSi220[pOD1249/pSW077; Pmex-5::GFP::tbb-2::operon_linker::mCHerry::his-11; cb-unc-119(+)]I; bub-1(syb1936,syb2383[bub-1(L282A;V285A,K718R;D847N)])I*	this study
bub-1(S283A); GFP::tubulin; mCherry::histone	FGP500	*bub-1(syb2396[bub-1((S283A)])I;ltSi220[pOD1249/pSW077; Pmex-5::GFP::tbb-2::operon_linker::mCHerry::his-11; cb-unc-119(+)]I*	this study
IFY-1::GFP; mCherry::histone	JAB222	*ify-1(erb-82[ify-1::linker::GFP])II;ltIs37[pAA64; pie-1p::mCherry::his-58; unc-119 (+)]IV; unc-119(ed3)???*	this study
IFY-1::GFP; mCherry::histone; *bub-1(L282A;V285A)*	FGP405	*ify-1(erb-82[ify-1::linker::GFP])II; ltIs37 [pAA64; pie-1p::mCherry::his-58; unc-119 (+)]IV; unc-119(ed3)???; bub-1(syb1936[bub-1(L282A;V285A)])I*	this study
GFP::MDF-1; mCherry::histone	OD2920	*unc-119(ed3)?III; ltIs37[pAA64; pie-1p::mCherry::his-58; unc-119 (+)]IV; mdf-1(lt39[gfp::tev::loxP::3xFlag::mdf-1])V*	Kim et al, 2017 (PMID: 28698300)
GFP::MDF-1; mCherry::histone; *bub-1(K718R;D847N)*	FGP434	*unc-119(ed3)?III; ltIs37[pAA64; pie-1p::mCherry::his-58; unc-119 (+)]IV; mdf-1(lt39[gfp::tev::loxP::3xFlag::mdf-1])V; bub-1(syb1746[bub-1((K718R;D847N)])I*	this study
GFP::MDF-1; mCherry::histone; *bub-1(L282A;V285A)*	FGP426	*unc-119(ed3)?III; ltIs37[pAA64; pie-1p::mCherry::his-58; unc-119 (+)]IV; mdf-1(lt39[gfp::tev::loxP::3xFlag::mdf-1])V; bub-1(syb1936[bub-1(L282A;V285A)])I*	this study
GFP::PAA-1; mCherry::histone	FGP438	*paa-1(syb2267[GFP::linker::paa-1]III; ltIs37[pAA64; pie-1p::mCherry::his-58; unc-119 (+)]IV*	this study
GFP::PAA-1; mCherry::histone; *bub-1(L282A;V285A)*	FGP388	*paa-1(syb2267[GFP::linker::paa-1]III; ltIs37 [pAA64; pie-1p::mCherry::his-58; unc-119 (+)]IV; bub-1(syb1936[bub-1((L282A;V285A)])I*	this study
GFP::PAA-1; mCherry::histone; bub-1(*K718R;D847N*)	FGP413	*paa-1(syb2267[GFP::linker::paa-1]III; ltIs37 [pAA64; pie-1/mCHERRY::his-58; unc-119 (+)]IV; bub-1(syb1746[bub-1((K718R;D847N)])I*	this study
GFP::PAA-1; mCherry::histone; bub-1(*L282A;V285A;K718R;D847N*)	FGP443	*paa-1(syb2267[GFP::linker::paa-1]III; ltIs37 [pAA64; pie-1/mCHERRY::his-58; unc-119 (+)]IV; bub-1(syb1936,syb2383[bub-1(L282A;V285A,K718R;D847N)])I*	this study
GFP::PAA-1; mCherry::histone; bub-1(*S283A*)	FGP445	*paa-1(syb2267[GFP::linker::paa-1]III; ltIs37 [pAA64; pie-1/mCHERRY::his-58; unc-119 (+)]IV; bub-1(syb1936,syb2383[bub-1(bub-1(syb2396[bub-1((S283A)])I)])I*	this study
GFP::PAA-1; mCherry::histone; *pptr-2Δ*	FGP387	*paa-1(syb2267[GFP::linker::paa-1]III; ltIs37 [pAA64; pie-1/mCHERRY::his-58; unc-119 (+)]IV; pptr-2(ok1467)V*	this study
PPTR-1::GFP	OD3600	*pptr-1(lt89[pptr-1::gfp])V*	Kim et al, 2017 (PMID: 28698300)
PPTR-1::GFP; mCherry::histone	FGP344	*pptr-1(lt89[pptr-1::gfp])V; ltIs37 [pAA64; pie-1p::mCherry::his-58; unc-119 (+)]IV*	this study
PPTR-1::GFP; mCherry::histone; *bub-1(K718R;D847N)*	FGP349	*pptr-1(lt89[pptr-1::gfp])V; ltIs37 [pAA64; pie-1p::mCherry::his-58; unc-119 (+)]IV; bub-1(syb1746[bub-1((K718R;D847N)])I*	this study
PPTR-1::GFP; mCherry::histone; *bub-1(L282A;V285A)*	FGP350	*pptr-1(lt89[pptr-1::gfp])V; ltIs37 [pAA64; pie-1p::mCherry::his-58; unc-119 (+)]IV; bub-1(syb1936[bub-1((L282A;V285A)])I*	this study
PPTR-1::GFP; mCherry::histone; *san-1Δ*	FGP379	*pptr-1(lt89[pptr-1::gfp])V;ltIs37 [pAA64; pie-1p::mCherry::his-58; unc-119 (+)]IV; san-1(ok1580) I*	this study
PPTR-1::GFP; mCherry::histone; bub-1(*L282A;V285A;K718R;D847N*)	FGP400	*pptr-1(lt89[pptr-1::gfp])V; bub-1(syb1936,syb2383[bub-1(L282A;V285A,K718R;D847N)]I*	this study
PPTR-1::GFP; mCherry::histone; bub-1(*S283A*)	FGP441	*pptr-1(lt89[pptr-1::gfp])V; ltIs37 [pAA64; pie-1/mCHERRY::his-58; unc-119 (+)]IV; bub-1(syb2396[bub-1((S283A)])I*	this study
PPTR-2::GFP	OD3424	*pptr-2(lt91[pptr-2::gfp])V*	Kim et al, 2017 (PMID: 28698300)
PPTR-2::GFP; mCherry::histone	FGP317	*pptr-2(lt91[pptr-2::gfp])V; ltIs37[pAA64; pie-1p::mCherry::his-58; unc-119 (+)]IV*	this study
PPTR-2::GFP; mCherry::histone; *bub-1(K718R;D847N)*	FGP323	*pptr-2(lt91[pptr-2::gfp])V; ltIs37[pAA64; pie-1p::mCherry::his-58; unc-119 (+)]IV; bub-1(syb1746[bub-1((K718R;D847N)])I*	this study
PPTR-2::GFP; mCherry::histone; *bub-1(L282A;V285A)*	FGP324	*pptr-2(lt91[pptr-2::gfp])V; ltIs37[pAA64; pie-1p::mCherry::his-58; unc-119 (+)]IV; bub-1(syb1936[bub-1((L282A;V285A)])I*	this study
PPTR-2::GFP; mCherry::histone; *san-1Δ*	FGP380	*pptr-2(lt91[pptr-2::gfp])V; ltIs37[pAA64; pie-1p::mCherry::his-58; unc-119 (+)]IV; san-1(ok1580) I*	this study
PPTR-2::GFP; mCherry::histone; bub-1(*L282A;V285A;K718R;D847N*)	FGP398	*pptr-2(lt91[pptr-2::gfp])V; bub-1(syb1936,syb2383[bub-1(L282A;V285A,K718R;D847N)]I*	this study
PPTR-2::GFP; mCherry::histone; bub-1(*S283A*)	FGP447	*pptr-2(lt91[pptr-2::gfp])V; ltIs37 [pAA64; pie-1/mCHERRY::his-58; unc-119 (+)]IV; bub-1(syb2396[bub-1((S283A)])I*	this study
GFP::ASPM-1; mCherry::histone	EU2876	*or1935[GFP::aspm-1] I; itIs37[pie-1p::mCherry::H2B::pie-1 3'UTR + unc-119(+)] IV*	Connolly AA, et al. J (PMID: 26370499)
PPTR-2::GFP; mCherry::histone	FGP477	*pptr-2(lt91[pptr-2::gfp])V; bqSi189[lmn-1p::mCherry::his-58 + unc-119(+)]II*	this study
PPTR-2::GFP; mCherry::histone; *sgo-1Δ*	FGP478	*pptr-2(lt91[pptr-2::gfp])V; bqSi189[lmn-1p::mCherry::his-58 + unc-119(+)]II; sgo-1(fq48)IV*	this study
PPTR-1::GFP; mCherry::histone	FGP479	*pptr-1(lt89[pptr-1::gfp])V; bqSi189[lmn-1p::mCherry::his-58 + unc-119(+)]II*	this study
PPTR-1::GFP; mCherry::histone; *sgo-1Δ*	FGP480	*pptr-1(lt89[pptr-1::gfp])V; bqSi189[lmn-1p::mCherry::his-58 + unc-119(+)]II; sgo-1(fq48)IV*	this study

Markers / *mutants*	Alelle	Primers (5'-3')	primer name	Restriction enzyme
bub-1(L282A;V285A); bub-1(L282A;V285A);(K718R;D847N)	*bub-1(syb1936[bub-1((L282A;V285A)])I; bub-1(syb1936,syb2383[bub-1 (L282A;V285A,K718R;D847N)]I*	ATGGAATATCGATTGAGGAGTTTC	fgp_153	*NsiI*
		CAATTTCGGGTTGTACTTCAGA	fgp_154	
bub-1(S283A)	*bub-1(syb2396[bub-1((S283A)])I*	ATGGAATATCGATTGAGGAGTTTC	fgp_153	*HhaI*
		CAATTTCGGGTTGTACTTCAGA	fgp_154	
bub-1(K718R;D847N)	*bub-1(syb1746[bub-1((K718R;D847N)])I*	GATGTGTCTTGTGCGTCCTC	fgp_125	*BmrI*
		CCAGTCCGGAAGTGAATCA	fgp_126	
pptr-2Δ	*pptr-2(ok1467)V*	ATCCTTGCTAAGCACAGTTGAAGT	fgp_137	
		CGTGAACGTGACTTTCTGAAGA	fgp_138	
san-1Δ	*san-1(ok1580) I*	GAAACTGCACGCTTAAAGCTTG	fgp_139	
		CTTTCCACGTTTCCCGTATC	fgp_140	
		GGGTGATTCGGCAGAAGA	fgp_141	
PPTR-1::GFP	*pptr-1(lt89[pptr-1::gfp])V*	CCTCGGAGAGTACACAAGACC	fgp_158	
		TGGAGTTGTCCCAATTCTTGTT	fgp_2	
		AGCAGCAGAAGACGAGAGAGT	fgp_159	
PPTR-2::GFP	*pptr-2(lt91[pptr-2::gfp])V*	ACGCCCTCAAGATGTTCAT	fgp_160	
		TGGAGTTGTCCCAATTCTTGTT	fgp_2	
		ACTGGGTAAGGAAGTCGAATCA	fgp_161	
AID::GFP::GSP-2	*gsp-2(syb545[AID::gfp::gsp-2])III*	TCTAATTGGGTTGTTTGAGCG	fgp_53	
		TGGAGTTGTCCCAATTCTTGTT	fgp_2	
		TTTTCCCTGGTTTGGATCC	fgp_54	

Supplementary Table 3. List of primers used for genotyping.